Distribution Agreement

In presenting this thesis as a partial fulfillment of the requirements for a degree from Emory University, I hereby grant to Emory University and its agents the non-exclusive license to archive, make accessible, and display my thesis in whole or in part in all forms of media, now or hereafter now, including display on the World Wide Web. I understand that I may select some access restrictions as part of the online submission of this thesis. I retain all ownership rights to the copyright of the thesis. I also retain the right to use in future works (such as articles or books) all or part of this thesis.

Valerie Linck April 4th, 2018

Cholesterol-dependent microvilli mediate the interaction of ENaC and PIP_2

by

Valerie Linck

He-Ping Ma
Adviser

Department of Biology

He-Ping Ma

Adviser

Douglas Eaton

Committee Member

Anita Corbett

Committee Member

2018

Cholesterol-dependent microvilli mediate the interaction of ENaC and PIP_2

By

Valerie Linck

He-Ping Ma

Adviser

An abstract of
a thesis submitted to the Faculty of Emory College of Arts and Sciences
of Emory University in partial fulfillment
of the requirements of the degree of
Bachelor of Sciences with Honors

Department of Biology

2018

Abstract

Cholesterol-dependent microvilli mediate the interaction of ENaC and PIP_2
By Valerie Linck

Epithelial sodium channels (ENaC) in the distal nephron play an important role in the regulation of total body Na^+ homeostasis. Gain-of-function mutations of ENaC, as seen in Liddle's syndrome, and hypercholesterolemia are both associated with hypertension. However, it is not clear how cholesterol can induce ENaC activation to result in hypertension. We know from previous studies that cholesterol stimulates ENaC in cultured distal nephron cells. In addition, we have shown that anionic phospholipids, including phosphatidylinositol 4,5-bisphosphate (PIP_2), can bind and stimulate ENaC in cultured distal nephron cells. We have also previously shown through atomic force microscopy studies that ENaC is mainly located in microvilli, which are cholesterol-dependent structures on the apical membrane of epithelial nephron cells. Likewise, we have also shown in the cortical collecting duct (CCD) that PIP_2 is predominantly located in microvilli and that PIP_2 distribution between microvilli and planar region depends on cholesterol synthesis. In the inner leaflet, it has been suggested that cholesterol may also interact with PIP_2 to form PIP_2 microdomains or to localize PIP_2 in lipid rafts. However, it is unclear whether ENaC and cholesterol are also co-localized in microvilli and, whether cholesterol affects the microvillar localization of PIP_2 and ENaC. *In vivo* results show that increasing cholesterol, through the blockade of the cholesterol regulating proteins, ABC-binding cassette transporter A1 (ABCA1) or apolipoprotein E (ApoE), induces hypertension. Furthermore, this hypertension may be alleviated through cholesterol synthesis inhibition. The blockade of ABCA1 also results in increased ENaC activity, which can be alleviated by cholesterol synthesis inhibition. The mechanism that mediates this hypertension is further elucidated by our *in vitro* studies. First, we show that ENaC activity is dependent on both cholesterol and PIP_2. Next, we show that the

structure of microvilli are dependent on cholesterol, and extraction of cholesterol or synthesis inhibition destroys microvillar structure. Furthermore, ENaC and PIP_2 both localize to the microvilli and each other in a cholesterol-dependent manner. Collectively, these results indicate that microvilli are cholesterol-dependent structures in which ENaC and PIP_2 colocalize to promote ENaC activation. An excess of cholesterol may result in ENaC-mediated hypertension by allowing an increase in microvillar domains and increased ENaC activation.

Cholesterol-dependent microvilli mediate the interaction of ENaC and PIP_2

By

Valerie Linck

He-Ping Ma

Adviser

A thesis submitted to the Faculty of Emory College of Arts and Sciences
of Emory University in partial fulfillment
of the requirements of the degree of
Bachelor of Sciences with Honors

Department of Biology

2018

Acknowledgements

First and foremost, I would like to thank my research advisors, Dr. He-Ping Ma and Dr. Douglas C. Eaton for all of their help and guidance. I would like to thank my mentor, Dr. Li Zou for all of her support throughout my undergraduate research career. I would like to thank Qiang Yue for helping me understand and contributing single channel measurements of epithelial sodium channels to my work. I would like to thank Dr. Mingming Wu and Dr. Yujia Zhai for all the work they contributed to this project. I would like to thank Dr. Anita Corbett for her contributions as a member of my committee. Finally, I would like to thank my parents, Karl and Patricia, and my siblings, Benjamin, Samantha, and Alexander, for their constant support and encouragement.

Table of Contents

Introduction

The renal system maintains ion homeostasis

Among many functions, the renal system is responsible for maintaining a homeostatic balance of ions in the body. In the renal system, the kidneys perform this function by filtering blood to produce a filtrate with the same electrolyte and water composition as blood but without blood cells or blood proteins. The kidneys then process the filtrate by reabsorbing just enough electrolytes and water to keep body compositions constant in the face of varying input, while excreting excess electrolytes and water into the urine. However, pathological excess reabsorption of certain ions, in particular, sodium, also causes an excess reabsorption of water. This imbalance increases overall blood volume, exerting greater pressure on the elastic vasculature and thus increasing blood pressure. Over time, chronically high blood pressure causes damage to or even failure of the kidneys as well as the heart and vasculature and can lead to stroke [1].

The kidneys accomplish filtration though millions of nephrons, the functional unit of the kidney (Fig. 1B). Nephrons pass through both the cortex and medulla of the kidney, regions which are both macroscopically visible on a renal cross section. Blood is first filtered through the renal corpuscle into the tubule of the nephron. The tubule contains many different segments and ion channels to allow proper filtration of ions and wastes. In the final, distal region of the nephron, the collecting duct, several nephrons merge together. The upper portion of this region, termed the cortical collecting duct (CCD), is responsible for fine-tuning the final salt concentration of the urine and, in turn, the total sodium balance of the body. Special epithelial cells in this region, principal cells, contain epithelial sodium channels (ENaC), which are sodium

channels that allow reabsorption from the urine back into the body to control sodium homeostasis [1].

ENaC is responsible for Na^+ homeostasis

ENaC in the distal nephron plays an important role in the regulation of total body Na^+ homeostasis. ENaC is assembled from homologous gene products mainly encoding α, β, and γ subunits[2] (Fig. 1A). Gain-of-function mutations of ENaC cause hypertension, as seen in Liddle's syndrome [3, 4]. Therefore, any physiological or pathological factors that stimulate ENaC should cause sodium retention resulting in volume-expanded hypertension [5-7]. Hypercholesterolemia, high plasma cholesterol, is also often associated with hypertension. These two facts have encouraged investigators to examine a possible role of cholesterol in regulating ENaC.

Cholesterol stimulates ENaC

Recently, we have shown that cholesterol, which constitutes more than thirty percent of the cell membrane lipid, stimulates ENaC in cultured distal nephron cells [8]. However, cholesterol is tightly packed with other membrane lipids in the apical membrane of epithelial cells. Our previous studies have shown that endogenous cholesterol is difficult to extract from the apical membrane of distal nephron cells and that exogenous cholesterol is also difficult to incorporate into the apical membrane [8]. Due to these difficulties, previous studies showed that attempts to manipulate cholesterol in the outer leaflet of the cell membrane at most only slightly affected ENaC activity [9, 10]. Therefore, for a long time, the question of whether cholesterol could regulate ENaC under physiological conditions has remained controversial. However, cholesterol is not only located in the outer leaflet, where it is resistant to experimental manipulations, but is also located in the inner leaflet. Whether the cholesterol in the inner leaflet is more important for

ENaC activity than that in the outer leaflet is not known.

Cholesterol can be regulated through ABCA1 and ApoE

Cholesterol in the inner leaflet is precisely controlled by the cholesterol transporter ATP-binding cassette transporter A1 (ABCA1) [11]. ABCA1 moves cholesterol from the inner membrane leaflet to the outer leaflet. Therefore, loss of ABCA1 function should lead to accumulation of cholesterol in the inner leaflet. If cholesterol in the inner leaflet regulates ENaC, manipulation of ABCA1 function should alter ENaC activity. Indeed, we have recently shown that pharmacological blockade of ABCA1 with cyclosporin A (CsA) or 4,4′-diisothiocyanostilbene-2,2′-disulfonic acid (DIDS) does elevate intracellular cholesterol and stimulate ENaC in cultured distal nephron cells [12]. These *in vitro* studies suggest that loss of ABCA1 cholesterol transporting function may cause hypertension by stimulating ENaC. However, in addition to inhibiting ABCA1, CsA also inhibits calcineurin [13], and DIDS also blocks other transporters and channels beyond ABCA1 [14]. Therefore, additional *in vivo* experiments are required to confirm that inhibiting ABCA1 reduces intracellular cholesterol and, thereby, regulates ENaC activity. These studies are significant because recent clinical studies suggest that loss of ABCA1 function due to reduced expression levels or loss-of-function polymorphisms correlates with hypertension [16, 17]. However, there is no direct evidence to show whether and how loss of ABCA1 function causes hypertension.

Cholesterol levels can also be modulated by the deletion of apolipoprotein E (ApoE). ApoE is responsible for removing excess cholesterol from the outer leaflet to be cleared [15]. Therefore, a combination of ApoE and ABCA1 blockade should produce a more severe hypercholesteremia model than blocking the action of either protein alone. Such experiments may further elicit

insights about the role of cholesterol in blood pressure regulation.

Microvilli are cholesterol dependent

As a major membrane component, cholesterol plays a critical role in regulating membrane fluidity and structure. The apical membrane of nephron epithelial cells contains protrusions called microvilli to increase the surface area presumably to enhance its transporting ability across the membrane. Scanning ion conductance and atomic force microscopy studies show that distal nephron A6 cells have extensive microvilli [18, 19]. Atomic force microscopy studies also suggest that ENaC is mainly localized within the microvilli [19]. This observation requires further investigation because localization was only based on an antibody to detect ENaC whose specificity was not well characterized. Another provocative observation is that extraction of cholesterol out of the outer leaflet of the apical membrane with the cholesterol sequestering agent, MβCD, induces Madin-Darby canine kidney cells to lose their microvilli [20]. We have recently shown that MβCD can also excise the microvilli of CCD principal cells to release vesicles from the apical membrane [21]. These studies together suggest a hypothesis that depletion of the outer leaflet cholesterol may reduce ENaC density by destruction of the microvilli. We have also shown that inhibition of cholesterol efflux from the inner leaflet of A6 cell apical membrane with ABCA1 transporter inhibitors increases intracellular cholesterol and ENaC activity [22]. Therefore, cholesterol may not only affect ENaC density via its outer leaflet localization, but may also regulate ENaC activity via its inner leaflet localization.

PIP_2 is necessary for ENaC activation

Several lines of evidence have shown that anionic phospholipids in the inner leaflet of the plasma membrane, especially PIP_2, stimulate ENaC [23-25]. Anionic phospholipids, including PIP_2,

can bind to all three ENaC subunits and directly stimulate ENaC in distal nephron A6 cells by allowing the negatively charged phospholipid to interact with positive residues on ENaC subunits [26, 27]. The apical membrane of CCD principal cells consists of two morphological domains: microvillar and planar regions. Recently, we have also shown that PIP_2 is predominantly located in microvilli and that PIP_2 distribution between microvilli and planar region depends on cholesterol synthesis in the CCD cells [21]. Cholesterol is localized both in the outer leaflet and in the inner leaflet of the plasma membrane. In the outer leaflet, cholesterol interacts with sphingolipids via hydrogen bonds to form membrane microdomains, also referred as lipid rafts [28-30]. Atomic force microscopy shows that the rafts in artificial membranes require cholesterol [31, 32]. In the inner leaflet, however, it has been suggested that cholesterol may also interact with PIP_2 to form PIP_2 microdomains or to localize PIP_2 in lipid rafts [33-35]. However, there are technical limitations in the determination of PIP_2 microdomains. First, lipid rafts or microdomains are nanometer-sized structures that are continuously changing size and extent [36, 37, 29]. Second, PIP_2 is located in the inner leaflet, which is inaccessible in intact cells. In contrast, the determination of PIP_2 distribution between microvilli and planar region is feasible. PIP_2 is predominantly localized in microvilli [21]. However, it is unclear whether ENaC and cholesterol are also localized in microvilli and, if so, whether cholesterol affects the microvillar localization of PIP_2 and ENaC.

Study Aims

In this report, we aim to test several hypotheses about how cholesterol and PIP_2 are linked to ENaC activation and total body sodium regulation. Using animal models in which *Abca1* and *Apoe* have been genetically deleted, as well as a pharmacological blockade of ABCA1, we examine the effect of altering cholesterol on systolic blood pressure and ENaC activity.

Furthermore, in vitro, we examine further the effect of cholesterol and PIP_2 on ENaC activity. We examine the localization of PIP_2, ENaC, and microvilli and the colocalization of ENaC and PIP_2 as well as PIP_2 and cholesterol. Our results show that microvilli are cholesterol-dependent structures that allow ENaC and PIP_2 to colocalize to promote PIP_2 mediated activation of ENaC. Furthermore, excess cholesterol may create may promote an increased number of microvillar domains, allowing increased sodium reabsorption and consequent hypertension, and defining a clear role of the kidney and ENaC in cholesterol induced hypertension.

Materials and Methods

Animals

All animal protocols and procedures were approved by the Animal Care and Use Committee of Emory University and were conducted in accordance with the Guide for the Care and Use of Laboratory Animals published by the National Institutes of Health.

Aqp2-cre and *Abca1-flox* mouse strains were purchased from The Jackson Laboratory (Maine, USA) as well as *Apoe* knockout (KO) mice, and colonies were established at Emory University. Conditional targeting of the mouse *Abca1* gene was achieved by flanking exons 45–46, which encode the second nucleotide-binding fold, with loxP sites as previously described [39]. The mice with a floxed *Abca1* gene were crossed with mice expressing Cre downstream of the *Aqp2* promoter. The *Aqp2-cre* gene has shown to be expressed only in the principal cells of the collecting duct, testis, and vas deferens [40]. To avoid possible complications from removal of *Abca1* from the vas deferens and testis, only female *Aqp2-cre* mice were used for breeding. Female homozygous *Aqp2-cre* mice were mated with male homozygous floxed *Abca1* mice. Females from the F1 generation were mated to homozygous male floxed *Abca1* mice to result in an F2 generation where 1/8 of the pups were heterozygous for *Aqp2-cre* and homozygous for floxed *Abca1*. These mice were used for experiments. Littermates without *Cre* but homozygous for floxed *Abca1* were served as the control. Mice will be genotyped by removing toes at day 10, and DNA will be extracted using a Quiagen DNeasy kit, and performing PCR using published primer sequences. The primer *Abca1* 13F (5'-GGA GGT GAC TGA AAG GCA TCC ATC), *Abca1* (CCT GTC TCA GCC CTG CAT GC-3') amplifies the region in the targeted allele spanning the loxP sites. The PCR product of the nonrecombined allele is 1600-bp, whereas the

recombined allele yields a 500-bp product. PCR amplified for the *Aqp2-cre* transgene using the primers *hAqp2* F2 (5′-AGT CAG AGA GAT GGG GGC CGG-3′) and CreTag R (5′-GCG AAC ATC TTC AGG TTC TGC GG-3′), which amplify the 730-bp junction between the *Aqp2* promoter and the *Cre* gene [41].

All animal experiments were performed using mice aged 3-5 months, and mice were housed in a temperature-controlled environment (23 ± 2°C) with a 12-h light/dark cycle. For evaluation of lovastatin's effect on *Abca1* KO mice, animals were divided into control mice and *Abca1* KO mice groups. After baseline systolic blood pressure measurement, mice received lovastatin (20 mg/kg/day) by intraperitoneal injection for another 4 weeks. For evaluation of lovastatin effects on CsA treated mice, wild type C57BL/6 mice were randomly divided into four groups and assigned to receive one of the following treatments for 4 weeks: (i) control (Kolliphor EL, 1 mL/kg/day, intraperitoneal), (ii) CsA (20 mg/kg/day, intraperitoneal), (iii) CsA (20 mg/kg/day, intraperitoneal) + Lovastatin (20 mg/kg/day, intraperitoneal), and (iv) Lovastatin (20 mg/kg/day, intraperitoneal). Kolliphor EL is a non-ionic emulsifier used to dissolve lipid soluable drugs. For evaluation of high fat diet effects on wild type C57BL/6 mice, mice were divided two groups: (i) 60% high fat diet and (ii) normal diet. For evaluation of CsA and high fat diet effects on *Apoe* KO animals, mice were divided into four groups: (i) normal diet, (ii) 60% high fat diet, (iii) CsA (20 mg/kg/day intraperitoneal), and (iv) CsA (20 mg/kg/day intraperitoneal) + 60% high fat diet. After baseline systolic blood pressure measurement, the mice were given ad libitum access to water and normal chow (Rodent Diet 5001; Lab Diet, Brentwood, MO, USA) or a high-fat diet (TD.06414 Adjusted Calories Diet 60/Fat; ENVIGO, Harlan Laboratories, Madison, WI, USA) continuously for 4 weeks.

Single-channel Patch Clamp *ex vivo*

Patch clamp electrophysiology was used to assess ENaC activity in isolated, split-open mice cortical collecting duct segment as previously described [42]. Single-channel ENaC currents were recorded in a cell-attached configuration with an Axon Multiclamp 200B amplifier (Axon Instruments, Foster City, CA, USA) at room temperature (22–25°C). The cortical collecting ducts were adhered to a cover glass coated with Cell-Tak (Corning, New York, NY, Cat. No.354240), and the cover glass was placed on a chamber mounted on an inverted microscope. The tubule was superfused with a bath solution containing (in mM) 140 NaCl, 5 KCl, 1 $CaCl_2$, and 10 HEPES adjusted to pH 7.4 with NaOH. Patch pipettes were pulled from borosilicate glass with a Sutter P-97 horizontal puller (Sutter, Novato, CA, USA), and the resistance of the pipettes ranged from 6 to 8 MΩ when filled with the pipette solution (in mM) 140 LiCl, 5 KCl, 1 $CaCl_2$, and 10 HEPES adjusted to pH 7.4 with NaOH. To assess the ENaC activity, patches were clamped to a potential of −40 mV and channel activity was determined during an at least 15-minute recording period. Only the patches with a seal resistance >2 GΩ were used. Data were sampled at 5 kHz with a low-pass filter at 1 kHz using Clampex 10.2 software (Molecular Devices, Sunnyvale, CA, USA). Before analysis, the single-channel traces were further filtered at 50 Hz. The single-channel amplitude was constructed by all-point amplitude histogram, and the histograms were fit using multiple Gaussians and optimized using a simplex algorithm. NP_O, the product of the number of channels and the open probability (Po), was used to measure the channel activity within a patch. When multiple channel events were observed in a patch, the total number of active channels (N) in the patch was determined.

Immunohistochemistry

Kidneys were fixed with 4% paraformaldehyde. For paraffin embedding, tissues were dehydrated in a series of graded ethanol followed by xylene and embedded in paraffin, and then

cut into 3-μm sections. Sections were deparaffinized and rehydrated. To reveal antigens, sections were incubated in 1 mM Tris solution (pH 9.0) supplemented with 0.5 mM EGTA and heated in a microwave oven for 5 min. Nonspecific binding of IgG was prevented by incubating the sections with 1% BSA for 30 min. Sections were incubated overnight at 4 °C with primary antibodies diluted in PBS supplemented with 1% BSA. The sections were washed in PBS-T and incubated with Alexa Fluor 488 conjugated donkey anti-rabbit IgG (A21206, 1:1000; Invitrogen) or Alexa Fluor 568 conjugated donkey anti-goat (A11057, 1:1000; Invitrogen) for 1 hr. For filipin staining, frozen kidney sections were fixed in 4% paraformaldehyde and then incubated with 1.5 mg/ml glycine. The kidney sections were incubated overnight at 4 °C with AQP2 antibody and then with Alexa Fluor 568 conjugated donkey anti-goat for 1 hr at room temperature. After washing with PBS, filipin was incubated for 1 hour at room temperature. Kidney sections were mounted with vectashield antifade mounting medium (Cat. Number: H-1000; Vectashield; Vector Laboratories). Filipin staining was viewed by confocal microscope using DAPI filter. All slides were imaged using a confocal microscope (Olympus, Fluoview1000, Japan). Identical acquisition settings were used for all images.

Western Blotting

Freshly isolated kidney cortex were minced and washed once with PBS and then homogenized using an Omni TH homogenizer (Warrenton, VA) with HEENG buffer [43] containing protease and phosphatase inhibitors (#1861280; Thermo Scientific). Tissue lysates were centrifuged at 1,000 rpm at 4°C for 10 min to remove debris. Protein concentration was determined using the BCA protein assay (cat 23223, cat 23224; Thermo Scientific). Forty micrograms of total protein were separated on 10% SDS-polyacrylamide gels and transferred onto polyvinylidene difluoride (PVDF) membranes, blocked by 5% nonfat dry milk or 3% fat

free bovine serum albumin (BSA) for 1 hour, followed by incubating with primary antibody for overnight. After washing with TBS-T, the membranes were incubated with horseradish peroxidase-conjugated goat anti-rabbit IgG secondary antibody (Bio-Rad, catalogue # 170-6515; 1:3000 dilution, Hercules, CA, USA) for 1 hour, labeled proteins were visualized with enhanced chemiluminescence (ECL) (Bio-Rad, catalogue # 170-5061, Hercules, CA, USA) and quantified by scanning densitometry (Bio-Rad). The intensities of bands of interest were normalized by the intensity of GAPDH (sc-25778, 1:1000 dilution) bands. Quantification of each band was performed via densitometry using the Image J software.

Antibodies

The antibodies used in this study were as follows: rabbit anti-ABCA1 (immunofluorescence 1:100； Western blots, 1:1,000， SAB4300712; Sigma Aldrich), goat anti-AQP2 (immunofluorescence 1:100, sc-9882; Santa Cruz Biotechnology), rabbit anti-α-ENaC (immunofluorescence 1:100； Western blots, 1:1,000， SPC-403; Stressmarq Biosciences).

Systolic Blood Pressure Measurements

Systolic blood pressure was measured by tail cuff, as previously described [44]. Data from the first day of each blood pressure cycle were discarded as this was considered a transition period in which the mice become accustomed to the procedure. Blood pressure was measured on a warmed platform (BP-2000, Visitech Systems), and mice were allowed to rest on the platform for 15 min before measurement. Five preliminary measurements were made and discarded to accustom mice to the procedure. Systolic blood pressure is an average of 10 measurements each day.

Cell Culture

Xenopus A6 distal nephron cells were purchased from American Type Culture Collection (Rockville, MD) and cultured as we previously reported [45]. The medium contained 2 parts of DMEM/F-12 (1:1) medium (Invitrogen), 1 part of H_2O, 15 mM $NaHCO_3$ (total Na^+ = 101 mM, which is ideal for amphibian A6 cells), 2 mM L-glutamine, 10% fetal bovine serum (Invitrogen), 25 μ/ml penicillin, 25 μ/ml streptomycin. A6 cells were cultured in plastic flasks in the presence of 1 mM aldosterone at 26° C and 4% CO_2. After the cells became 70% confluent in plastic flasks, A6 cells were plated on the polyester membrane of either Snapwell inserts (Corning Costar Co) for patch-clamp experiments or Transwell inserts (Corning Costar Co) for confocal microscopy experiments and measurement of amiloride-sensitive Na^+ current. The cells were cultured for two to three weeks to allow them to be fully polarized before each experiment. The mouse CCD principal cell line ($mpkCCD_{c14}$) [46] was also used in the study and cultured on Transwell inserts with permeable polyester membranes, as we previously reported [47]. Briefly, the $mpkCCD_{c14}$ cells were incubated in a 1:1 mix of DMEM/F12 medium (Invitrogen, Carlsbad, CA) supplemented with 50 nM dexamethasone, 1 nM triiodothyronine, 20 mM HEPES, 2 mM L-glutamine, 0.1% penicillin/streptomycin, and 2% heat inactivated FBS. Cells were maintained at 37º with 5% CO_2 in air for two to three weeks until forming a confluent monolayer and becoming fully polarized.

Patch-clamp Recordings *in vitro*

Both cell-attached and inside-out recordings of ENaC single-channel currents from A6 cells were carried out using an Axopatch 200B amplifier (Molecular Devices, Sunnyvale, CA). As previously described [22], prior to the experiments, A6 cells cultured on the polyester membrane of Snapwell inserts were thoroughly washed with NaCl solution containing (in mM):

100 NaCl, 3.4 KCl, 1 $CaCl_2$, 1 $MgCl_2$, and 10 HEPES; pH was adjusted to 7.4 with NaOH. The glass micropipette was filled with NaCl solution (the pipette resistance was ranged from 7 to 10MΩ). In cell-attached experiments, NaCl solution was used for the bath in the patch chamber. For experiments using the inside-out patch-clamp configuration, KCl solution was used for the cytoplasmic bath, which contained (in mM): 100 KCl, 5 NaCl, 1 $MgCl_2$, and 10 HEPES (50 nM free Ca^{2+} after titration with 1 mM EGTA); pH was adjusted to 7.2 with KOH. Single-channel currents were obtained with applied pipette potentials of either 0 mV for cell-attached recordings or +60 mV for inside-out recordings, filtered at 1 kHz, and sampled every 50 μs with Clampex 10.2 software (Molecular Devices, Sunnyvale, CA, USA). All experiments were conducted at room temperature (22-24ºC). The total numbers of functional channels in the patch were estimated by observing the number of peaks detected on the current amplitude histograms during at least 10 min recording period. Each experiment was started after the first 2-min recordings when the ENaC activity had stabilized. The open probability (P_O) of ENaC under control conditions and after each experimental manipulation was calculated using Clampfit 10.2 (Molecular Devices, Sunnyvale, CA, USA).

Transfection of mpkCCD$_{c14}$ Cells

In this set of experiments, mpkCCD$_{c14}$ cells were used because the transfecting efficiency of these cells was much higher than that of A6 cells. Therefore, mpkCCD$_{c14}$ cells were plated on the polyester membrane of Transwell inserts at a high density to allow the cells to be confluent within three days. Cells were incubated with DNA constructs of either enhanced green (or yellow) fluorescence protein (EGFP or EYFP)-tagged pleckstrin homology domain (PHD) of phospholipase C (PLC) d1 (EGFP-PHD-PLCd1 or EYFP-PHD-PLCd1, respectively) or enhanced cyan fluorescence protein (ECFP)-tagged α-ENaC (ECFP-α-ENaC) in the presence of

Lipofectamin 2000 for 6 h. The cells were then incubated with regular culture medium for two days before performing the confocal microscopy experiments.

Confocal and Atomic Force Microscopy Imaging

Olympus confocal microscope (FV-1000, Japan) was used. Prior to the confocal microscopy experiments, cells were washed twice with saline containing (in mM) 145 NaCl, 5 KCl, 1 $CaCl_2$, 1 $MgCl_2$ and 10 HEPES; adjusted pH to 7.4 with NaOH. To localize α-ENaC in microvilli, A6 cells were fixed with 4% paraformaldehyde for 15 min, permeabilized with 0.1% triton-X100 for 15 min, then incubated with α-ENaC antibody (SPC-403; Stressmarq Biosciences) followed with a secondary staining with Alexa Fluor 594 (5 mg/ml). To co-localize cholesterol with PIP_2 in the microvilli, the cells expressing EGFP-PHD-PLCd1 were fixed with 4% paraformaldehyde for 15 min and then staining with filipin for 15 min. To co-localize PIP_2 with α-ENaC in microvilli, live mpkCCD_{c14} cells expressing both EYFP-PHD-PLCd1 and ECFP-α-ENaC were used. The polyester membrane that supports the cell monolayer was excised and mounted on a glass slide either with a drop of NaCl solution for live cells or a drop of mounting solution for fixed cells. Confocal microscopy XY scanning of the cells at the microvillar level was accomplished within 5 min. XY optical sections were performed to provide a flat view of the cell surface at the microvillar level. For atomic force microscopy imaging, A6 cells were either under control conditions or treated with 50 mM MβCD for 30 min before the cells were fixed with 4% paraformaldehyde for 15 min. In each set of confocal or atomic force microscopy experiments, images were taken using the same parameter settings.

Chemicals

All chemicals for electrophysiological recordings were purchased from Sigma-Aldrich (St

Louis, MO) except when specified. CsA was purchased from Tocris (Ellisville, MO, USA).

Statistical Analysis

Data is reported as mean values ± SD or mean values ± SEM. Statistical analysis was performed with SigmaPlot and SigmaStat software (Jandel Scientific, CA). Student *t* test was used for comparisons between two groups whereas paired *t*-test was used for comparisons between pre and post treatment activities. Analysis of variance (ANOVA) was used for multiple comparisons among various treatment groups. Results were considered significant if $p < 0.05$.

Results

Modulating intracellular cholesterol alters systolic blood pressure

To determine whether modulating intracellular cholesterol affects blood pressure, the average basal systolic blood pressure was compared between several groups of mice under conditions to alter cholesterol. To eliminate the possible involvement of extracellular cholesterol, we also measured systolic blood pressure in the mice fed with either normal diet or high fat diet. The data show that high fat diet for 2 weeks did not alter systolic blood pressure (Fig. 2A). However, mice lacking ApoE did have significant increases in systolic blood pressure on a high fat diet after 1 week, which continued to week 4 (Fig. 3). Pharmacological blockade of ABCA1 with CsA also resulted in a significant increase in systolic blood pressure. Consistently, CsA-induced elevation of systolic blood pressure reversed by inhibiting intracellular cholesterol synthesis via lovastatin (Fig 2B). Furthermore, *Apoe* knockout mice treated with a high fat diet and CsA experienced more severe hypertension with a quicker onset. To test whether ABCA1 regulates ENaC, we crossed *Abca1* floxed mice with aquaporin 2 *(Aqp-2) cre* mice to selectively delete *Abca1* in CCD principal cells. To confirm that the deletion only occurs in CCD principal cells, we performed both confocal microscopy and Western blot assay. In control mice, ABCA1 was observed in most tubular cells including CCD principal cells. However, in the principal cell-selective *Abca1* KO mice, ABCA1 was only detected in the cells of other nephron segments, but not in the principal cells that express AQP-2 (Fig. 4A). The total ABCA1 protein in the kidney cortex was also significantly reduced in the principal cell-selective *Abca1* KO mice (Fig. 4B and 4C). The data show that systolic blood pressure of *Abca1* KO mice was significantly higher than that of control mice (Fig. 5). Interestingly, *Abca1*-KO-induced increase in systolic blood pressure was significantly reversed by lovastatin within two weeks, while lovastatin had no effect on

systolic blood pressure of control mice (Fig. 5). Since our previous studies have already shown that lovastatin, a cholesterol synthesis inhibitor, can significantly reduce cholesterol levels in cultured distal nephron cells [47], these data suggest that *Abca1* KO and CsA can elevate systolic blood pressure in mice and that the elevation can be corrected by lovastatin.

Deletion of ABCA1 in CCD principal cells elevates ENaC activity

Using the *Abca1* KO mice, we performed cell-attached patch-clamp experiments to examine ENaC activity in the split-opened CCD cells (Fig. 6A). The data demonstrate that deletion of *Abca1* significantly increased both ENaC open P_O from 0.19 ± 0.30 (Control mice) to 0.44 ± 0.06 (*Abca1* KO mice) and the number of active ENaC (*N*) from an average of 3 active channels per patch (Control mice) to an average of 5 active channels per patch (*Abca1* KO mice) (Fig. 6B-E). These results indicate that loss of ABCA1 function in CCD principal cells elevates ENaC activity. Furthermore, mice treated with lovastatin significantly decreased ENaC open P_O in *Abca1* KO mice from 0.44 ± 0.06 to 0.15 ± 0.03, indicating that reducing cholesterol can reverse the ENaC over activation in these mice (Fig. 6B-E).

Cholesterol stimulates ENaC in a PIP_2-dependent manner

To determine whether depletion of cholesterol reduces ENaC activity by decreasing PIP_2, we performed excised inside-out patch-clamp experiments. The data show that exposure of the inner leaflet of the patch membrane to only 0.5 mM MβCD, to extract cholesterol from the membrane, significantly reduced ENaC P_O and that the reduction was reversed by 30 μg/ml cholesterol (Fig. 7A and B). The concentration MβCD we used in this experiment to extract the cholesterol in the inner leaflet of the apical membrane is 100 times lower than what we used (50 mM) to extract cholesterol out of the outer leaflet, indicating that cholesterol in the inner leaflet

is relatively loose and that the effect of MβCD is more specific. To determine whether cholesterol alters ENaC activity via PIP_2, cholesterol was extracted out of the inner leaflet of the patch membrane with 0.5 mM MβCD, and we used an antibody to PIP_2 to sequester PIP_2 in the patch membrane. The data show that after ENaC activity was reduced by extraction of cholesterol in the patch membrane with MβCD, the addition of cholesterol no longer reversed the effects when PIP_2 was sequestered with its antibody (Fig. 8A and B). These results suggest that PIP_2 is required for cholesterol to stimulate ENaC.

PIP_2 and α-ENaC are localized in microvilli

We have recently shown that the ENaC activator, PIP_2, is located in microvilli and that its levels are regulated by lovastatin [21]. To determine whether acute extraction of membrane cholesterol can alter PIP_2 levels in microvilli, we performed confocal microscopy experiments. First, the cell surface image was obtained with differential interference contrast microscopy (DIC). The image shows that microvilli form a lirelliform structure on the cell surface. By merging the DIC image with the confocal microscopy image of PIP_2, we show that PIP_2 lined up along with microvilli and that after application of MβCD to the same cell, both microvilli and PIP_2 were no longer observed (Fig. 9A and B). Since PIP_2 stimulates ENaC via a direct interaction [23, 27] theoretically, ENaC should be also localized in microvilli. Indeed, the data show that the channel pore-forming subunit α-ENaC was mainly observed in microvilli (Fig. 10). From the zoom-in DIC image in Fig. 10 using a magnification two times higher than what used in Fig. 9, we noticed that each lirelliform structure contains several microvilli which fused in a line. This fact was clearly observed by scanning the cell surface with atomic force microscopy (Fig. 11). To confirm the effect of MβCD on microvilli which we observed in DIC images shown in Fig. 9, we treated the cells with 50 mM MβCD and then scanned the cell surface with atomic

force microscopy. The data show that MβCD almost completely eliminated the microvilli on the cell surface. These data suggest that acute extraction of cholesterol deconstructs microvilli and reduces PIP_2 in microvilli.

MβCD and lovastatin reduce α-ENaC and PIP_2 in the microvilli

To eliminate the possibility that the microvillar α-ENaC fluorescence detected by its antibody reflected a non-specific signal other than α-ENaC, live mpkCCD$_{c14}$ cells were used in the following experiments. Prior to the experiments, mpkCCD$_{c14}$ cells were co-transfected with DNA constructs encoding either ECFP-tagged α-ENaC to visualize α-ENaC or EYFP-tagged PH domain of PLCδ1 to visualize PIP_2. Confocal microscopy XY optical sections were performed at the live cell surface level. The data show that α-ENaC and PIP_2 are co-localized in microvilli (Fig. 12A). After treatment of the cells with 50 mM MβCD to extract the cholesterol in the outer leaflet of the cell membrane, the cyan fluorescent intensity, which represents the levels of α-ENaC, was significantly decreased, and the total yellow fluorescent intensity, which represents the levels of PIP_2, was also significantly decreased (Fig. 12B and C). Similarly, after treatment of the cells with 25 μM lovastatin to inhibit cholesterol synthesis in the cells, the fluorescent intensity which represents both α-ENaC and PIP_2 was significantly decreased (Fig. 13A-C). These data suggest that α-ENaC is co-localized with PIP_2 in microvilli via a cholesterol-dependent mechanism.

MβCD and lovastatin reduce cholesterol and PIP_2 in the microvilli

To determine if cholesterol is co-localized with PIP_2 in microvilli, we performed confocal microscopy XY optical sections using the mpkCCD$_{c14}$ cells transfected with plasma DNA containing EGFP-tagged PH domain of PLCδ1 to visualize PIP_2 and stained with filipin, a

fluorescent compound which can bind to cholesterol to visualize cholesterol. The data show that cholesterol is predominantly co-localized with PIP_2 in microvilli and that both cholesterol and PIP_2 were significantly reduced after treatment of the cells with 50 mM MβCD for 30 min (Fig. 14A-C). Similarly, after treatment of the cells with 25 μM lovastatin for 24 h both cholesterol and PIP_2 were significantly reduced (Fig. 15A-C). Since we have recently shown that the lipid rafts which are cholesterol-rich microdomains are mainly located in microvilli [21], these data suggest that CCD cells can synthesize cholesterol and that cholesterol accumulates in microvilli with PIP_2 to form a unique membrane microdomain to regulate ENaC activity.

Discussion

Increased intracellular cholesterol induces hypertension via ENaC

This study describes one mechanism by which increased intracellular cholesterol induces hypertension; that is, by increasing the activity of epithelial sodium reabsorption via epithelial sodium channels in the distal nephron. It also provides a mechanism that explains the clinical observation that one serious side effect of cyclosporin A is severe hypertension.

Besides these major findings concerning the role of cholesterol in regulating blood pressure, there are several interesting specific observations. First, the study shows that increasing extracellular cholesterol in wildtype mice through a high fat diet is not sufficient to increase blood pressure in the short term (4 weeks). However, blood pressure is increased if intracellular cholesterol is increased by inhibiting cellular extrusion by blocking ABCA1 with the immunosuppressive agent CsA. This effect is due to cholesterol since the cholesterol-induced hypertension can be alleviated by treatment with the cholesterol synthesis inhibitor, lovastatin.

While increasing intracellular cholesterol produces hypertension on all diets and increasing extracellular cholesterol does not, increasing extracellular cholesterol is not without consequences. Even though increasing extracellular cholesterol in wildtype mice does not increase blood pressure in wildtype mice, blocking cholesterol clearance, by knocking out *Apoe*, can cause hypertension in mice fed a high fat diet. In addition, when treated with CsA to block ABCA1, the *Apoe* knockout model had quicker hypertensive onset when coupled with a high fat diet and ultimately resulted in more severe hypertension in groups treated with CsA alone and CsA plus high fat diet. These results all indicate that CsA-induced hypertension is cholesterol dependent. While CsA provides a pharmacological block of ABCA1, we could provide the same

results in a more direct manner by genetically deleting *Abca1* in a CCD specific *Abca1* knockout mouse.

There are several potential sources of hypertension, but one possible mechanism is excess sodium in the distal nephron associated with elevated ENaC activity; and our measurements of blood pressure correlate with the activity of ENaC in the collecting tubules. The present study for the first time shows that deletion of *Abca1* increases ENaC activity (both the open probability, P_O, and channel density) in the apical membranes of principal cells in the cortical collecting duct. Furthermore, treating *Abca1* KO mice with lovastatin decreases ENaC P_O. In parallel to the elevated ENaC activity, we show that deletion of *Abca1* in principal cells does cause hypertension. Interestingly, lovastatin, a cholesterol synthesis inhibitor, can correct the *Abca1* KO-induced hypertension.

There is little question that the immunosuppressive drug CsA causes severe hypertension. Our data for the first time show that the hypertension induced either by CsA or by deletion of *Abca1* can be corrected by inhibiting cholesterol synthesis with lovastatin, indicating that CsA causes hypertension via a novel pathway associated with loss of ABCA1 function and accumulation of cholesterol in principal cells. Nevertheless, accumulation of cholesterol in principal cells due to loss of ABCA1 function should play an important role in CsA-induced hypertension because lovastatin can completely reverse the elevation of the blood pressure. Therefore, the present study is evidence for a possible clinical trial to examine whether lovastatin can be used as a treatment for CsA-induced hypertension.

ENaC and PIP_2 are localized to the microvilli

While our studies illustrate the role of cholesterol in hypertension *in vivo,* further *in vitro* studies were conducted to further understand the mechanism of this hypertension. The present study for the first time shows that ENaC is co-localized with its activator PIP_2 in the microvilli in a cholesterol-dependent manner. Three different approaches were used to manipulate cholesterol levels in the apical membrane of distal nephron cells. First, methyl-β-cyclodextrin (MβCD) was used to acutely extract the cholesterol in the outer leaflet of the plasma membrane. Second, lovastatin was used to inhibit cholesterol synthesis in the cells. Third, the cholesterol in the inner leaflet of the plasma membrane was directly manipulated in excised inside-out patches. Consistent with a recent report [21], we show that acute extraction of the cholesterol from the outer membrane leaflet can reduce microvilli. We also show that ENaC and PIP2 are localized in the specialized apical membrane forming the microvilli. Although a previous report has already suggested that ENaC may be located in microvilli [19], further studies are required because the suggestion is based on data using an antibody to ENaC, which has not been completely characterized. In the present study, we have used an antibody, which specifically binds to α-ENaC, and we have confirmed the results by expressing a fluorescence-tagged α-ENaC in the cells. Furthermore, our confocal microscopy data show that acute extraction of the cholesterol in the outer membrane leaflet can reduce α-ENaC density and PIP_2 levels in the apical membrane. The reduction appears to be caused by simply excising the microvilli where α-ENaC and its activator PIP_2 are located. In contrast, inhibition of cholesterol synthesis in the cells with lovastatin should mainly reduce the cholesterol in the inner leaflet of the plasma membrane because cholesterol flipping between the inner and outer membrane leaflets is rare, but can be facilitated by cholesterol-transporters such as ABCA1 [49, 50]. Furthermore, we show that short-

term treatment with lovastatin (24 h) does reduce cholesterol, PIP_2, and α-ENaC density in the microvilli.

Microvilli are cholesterol-dependent and allow ENaC and PIP_2 to associate

Our cell-attached patch-clamp data show that MβCD reduces the number of active ENaC in the patch by excising the microvilli and decreases ENaC P_O by decreasing PIP_2. We and others have previously shown that MβCD excises microvilli from the apical membrane in a manner similar to tremendously accelerated exocytosis [21, 51]. We argue that the remaining ENaC with lower activity after extraction of cholesterol may reflect the ENaC in the basal part of microvillar membrane, which is fused and flattened after the major exocytosis induced by MβCD. Reducing the cholesterol in the inner membrane leaflet by inhibiting cholesterol synthesis in the cells with lovastatin can produce similar effects on the number of active ENaC and ENaC P_O. However, the mechanism should be different because lovastatin does not excise the microvilli as MβCD does, but does decrease PIP_2 in the microvilli. Nevertheless, our inside-out patch-clamp experiments provide evidence to show that PIP_2 is required for cholesterol to increase ENaC P_O. Furthermore, the concentration of MβCD that is required to reduce ENaC P_O by extracting the cholesterol in the inner membrane leaflet is more than 100 times lower than the concentration that is required for extracting the cholesterol in the outer membrane leaflet to excise microvilli. The observation is not surprising because the cholesterol in the outer leaflet interacts with sphingolipids with long fatty acid chains via hydrogen bonds to form tightly packed microdomains, also referred as lipid rafts [28, 29]. Since the inner leaflet does not contain any sphingolipids, the cholesterol in the inner leaflet cannot be tightly packed to form lipid rafts. Therefore, it requires much less MβCD to extract cholesterol from the inner leaflet. Cholesterol in the inner leaflet is known to interact with PIP_2, which is associated with cytoskeleton [52, 53].

PIP_2 is a strong activator of ENaC [23, 24, 25]. We have shown that anionic phospholipids including PIP_2 can bind to all three ENaC subunits and directly stimulate ENaC in excised inside-out patches [27]. Therefore, the decreases of PIP_2 in microvilli where ENaC is located should account for the reduction of ENaC activity caused by depletion of cholesterol.

Summary: Cholesterol mediates the interaction of ENaC and PIP_2 via microvilli

Cholesterol is directly linked to hypertension through both the circulatory and renal system, with this report focusing on the latter. In the vasculature, cholesterol, mainly extracellular, forms plaques over many years leading to hardening and narrowing of vasculature inducing hypertension as well as further strain on the heart. However, this report establishes a clear link for a much more rapid mechanism for cholesterol-induced hypertension in the renal system. It is now clear that cholesterol is responsible for microvilli formation in epithelial cells of the cortical collecting duct. These microvilli allow ENaC to co-localize with its activator, PIP_2, to allow activation and sodium reabsorption (Fig. 16). Without cholesterol, there are less microvilli and less co-localization of ENaC and PIP_2. Furthermore, excess cholesterol may create more of these domains to allow ENaC and PIP_2 to co-localize and thus induce excess sodium reabsorption leading to hypertension. This study illustrates the mechanism of rapid cholesterol-induced hypertension in the renal system and provides, in the use of statins, a possible treatment for hypertension induced by this mechanism.

Figures

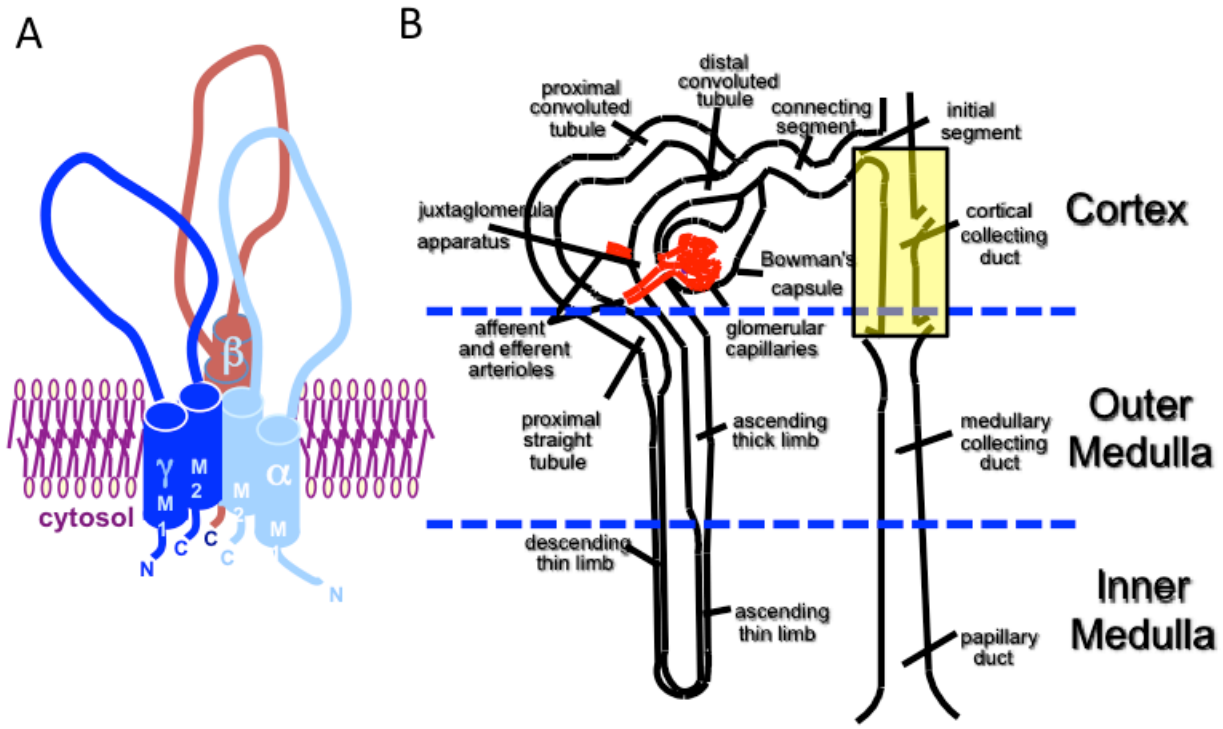

Figure 1. ENaC structure and anatomy of the human nephron. (A) Structure of ENaC showing the subunits interacting in the membrane. **(B)** Illustration to show the anatomy of the human nephron and its segments as labeled. The yellow box indicated the cortical collecting duct, our region of interest as it contains ENaC in the principal cells of this region.

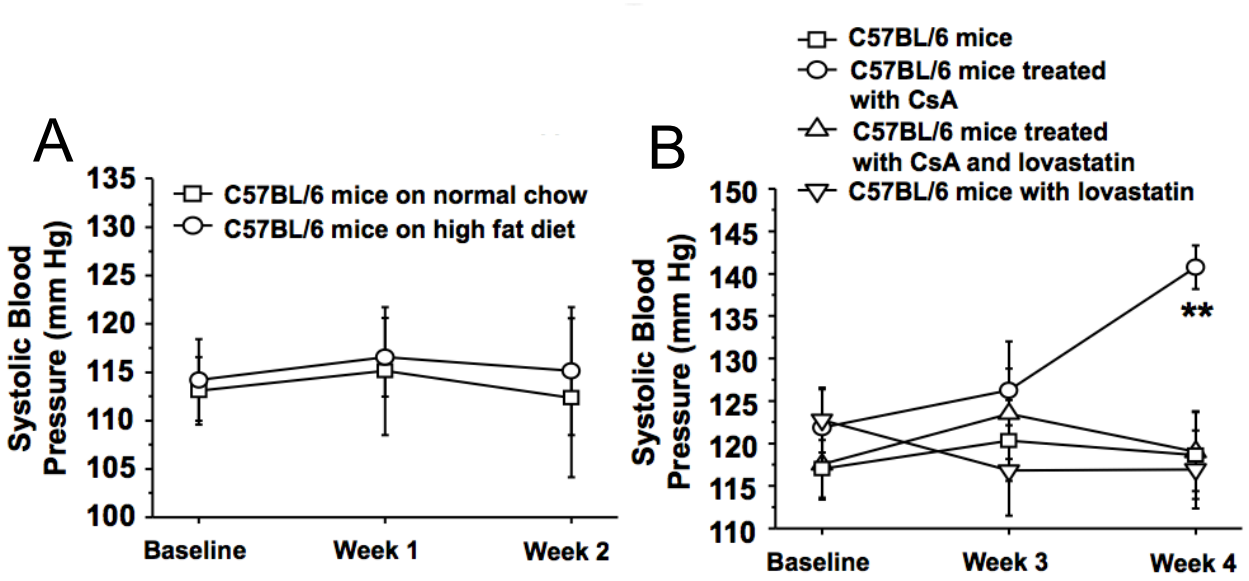

Figure 2. Pharmacological blockade of ABCA1 induces hypertension and can be alleviated by inhibiting intracellular cholesterol synthesis. (A) Systolic blood pressure (mmHg) from mice treated with high fat diet showed no significant difference compared with wild type C57BL/6 mice on normal diet. (n = 9 in each group). **(B)** Blood pressure from mice treated with CsA significantly increased compared with wild type C57BL/6 mice, while lovastatin attenuated the elevated blood pressure. (**$P < 0.01$, n = 4 in each group).

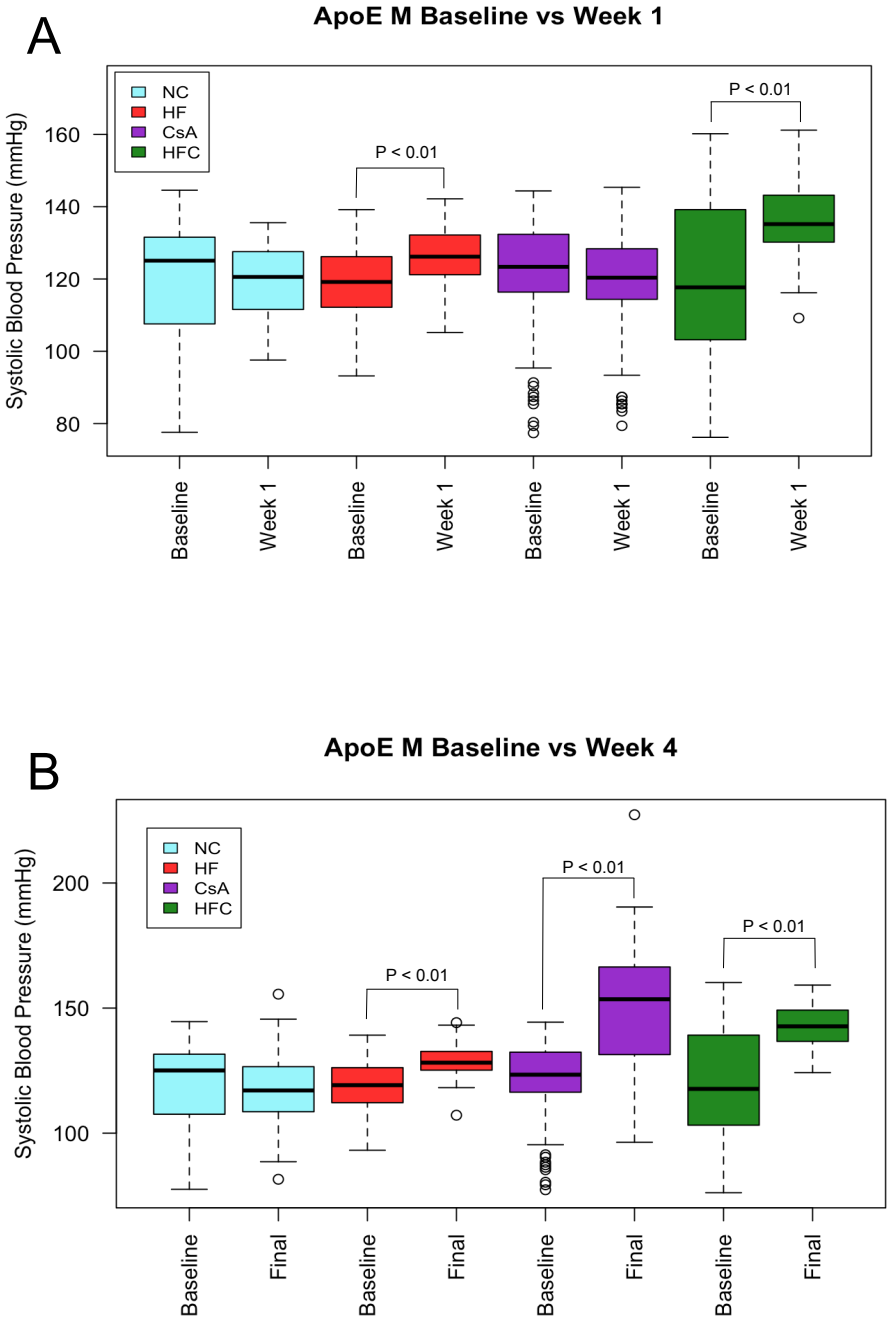

Figure 3. Deletion of ApoE induces faster onset of CsA-mediated hypertension. (A) Blood pressure from *Apoe* knockout male (M) mice treated with high fat diet or high fat diet plus CsA show significant blood pressure increases after one week of treatment as compared to *Apoe* knockout mice baseline measurements. (n = 4 in each group). **(B)** Blood pressure from *Apoe*

knockout mice treated with high fat diet, CsA, or high fat diet plus CsA all show significant increases in blood pressure from baseline measurements. (n = 4 in each group).

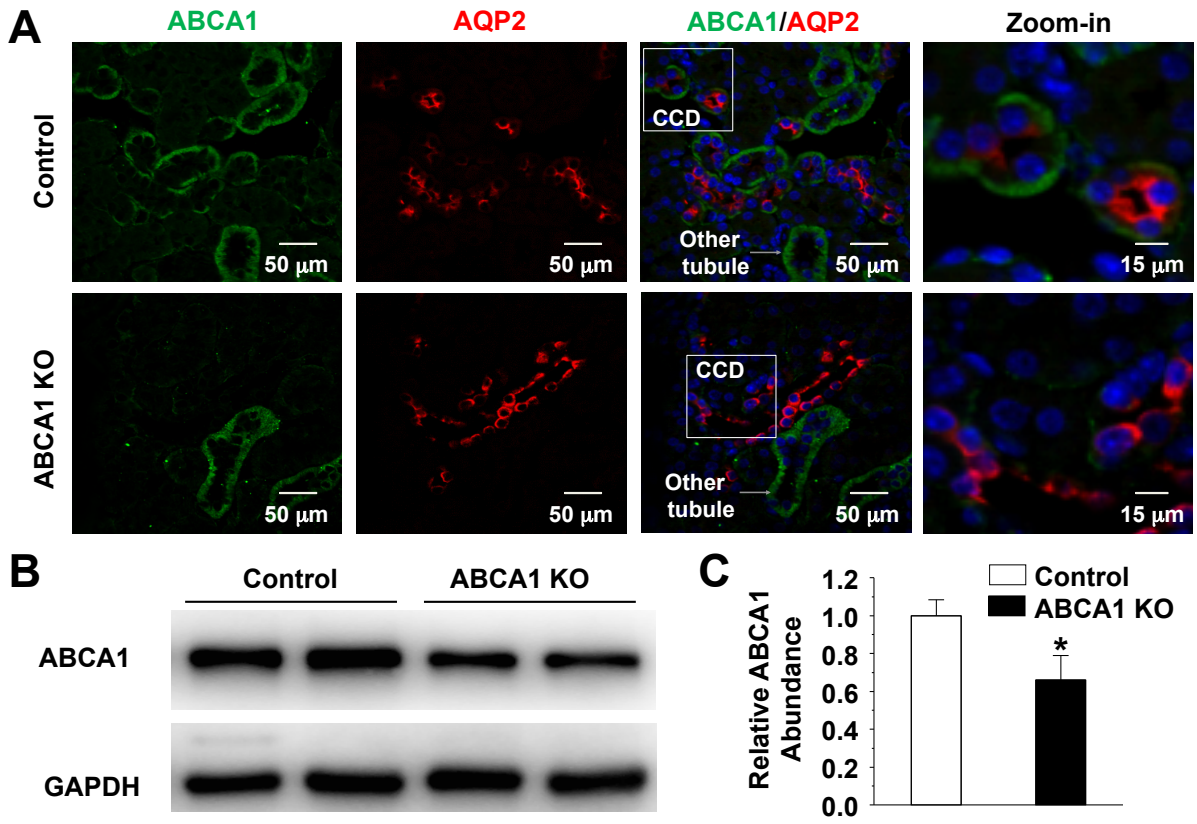

Figure 4. ABCA1 was specifically deleted in the principal cells of mouse cortical collecting duct. (A) Confocal microscopy images of ABCA1 (green) in control and *Abca1* KO mice. CCD was labeled with an anti-AQP2 antibody shown in red. Each experiment was repeated three times on each mouse. The images represent data from 4 mice, showing consistent results. **(B)** Western blot of kidney cortex lysates from control and *Abca1* KO mice using antibodies against ABCA1 and GAPDH as a loading control. **(C)** Summary plots of Western blots showing ABCA1 expression in kidney cortex from control and *Abca1* KO mice (*$P < 0.05$, n = 8 in each group). Figure provided by M. Wu.

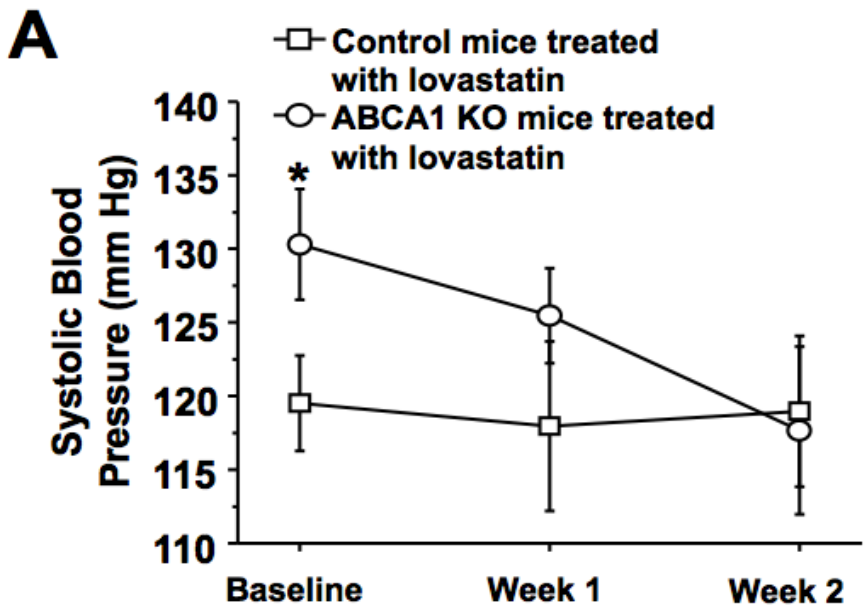

Figure 5. Lovastatin corrects hypertension caused by loss of ABCA1 function. (A) Blood pressure from *Abca1* knockout mice was significantly increased compared with paired control mice, while lovastatin attenuated the elevated blood pressure. (*$P < 0.05$, n = 15 in each group).

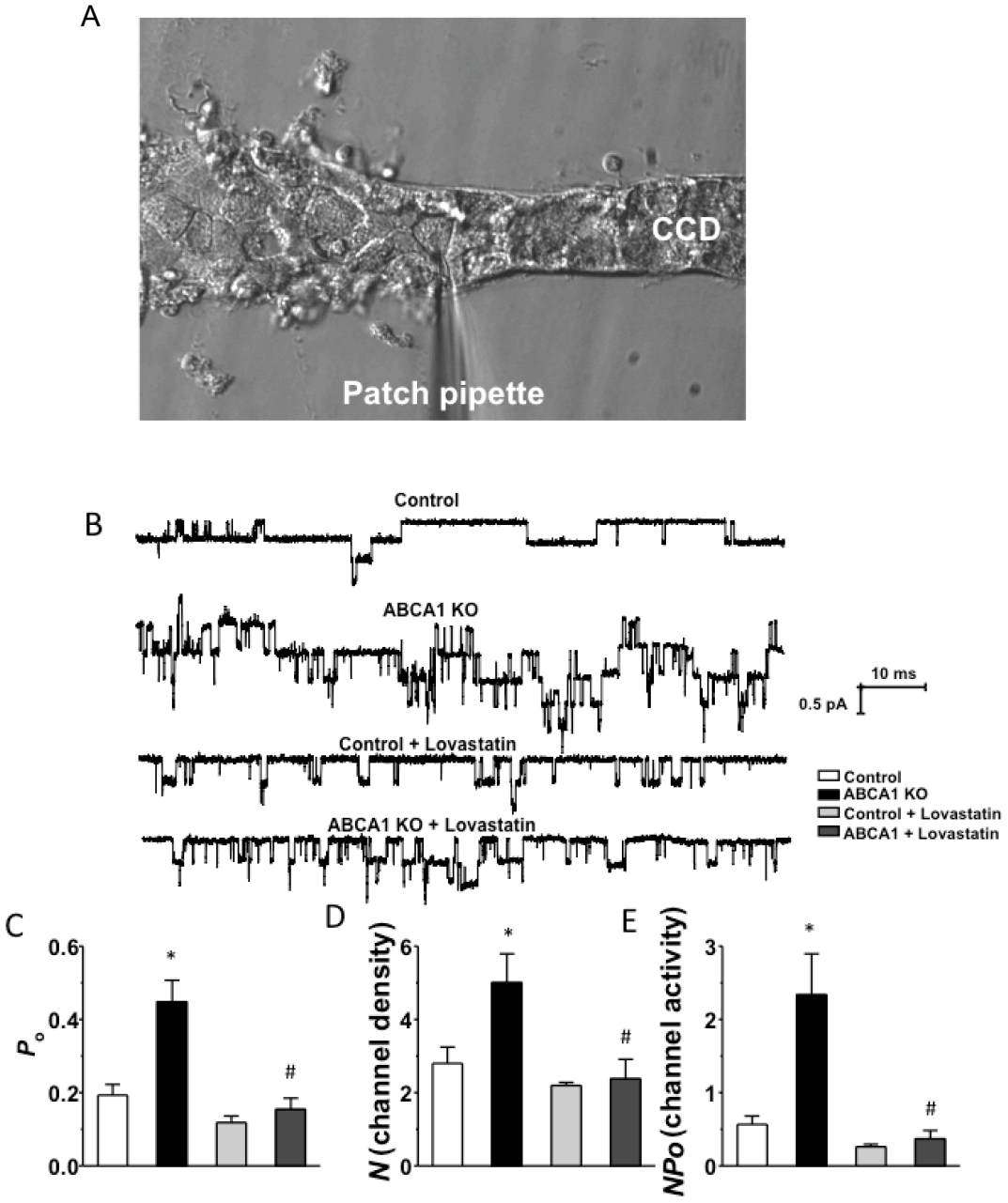

Figure 6. Lovastatin reduces both ENaC P_O and the number of active ENaC in the patch of *Abca1* KO mice. (A) A split-opened CCD for cell-attached patch-clamp recordings. **(B)** Representative single-channel recordings either from a wildtype mouse, *Abca1* KO mouse, control mouse treated with lovastatin, or *Abca1* KO mouse treated with lovastatin. Downward

events show ENaC openings. $V_{pipette}$ = +40 mV. **(C-E)** Summary plots of ENaC P_O (**C**), channel density (**D**), and $\boldsymbol{NP_O}$ **(E)**, which is N times P_O. (* = $P < 0.05$, difference between control and *Abca1* KO, # = $P < 0.05$, difference between control and *Abca1* KO and *Abca1* KO with lovastatin).

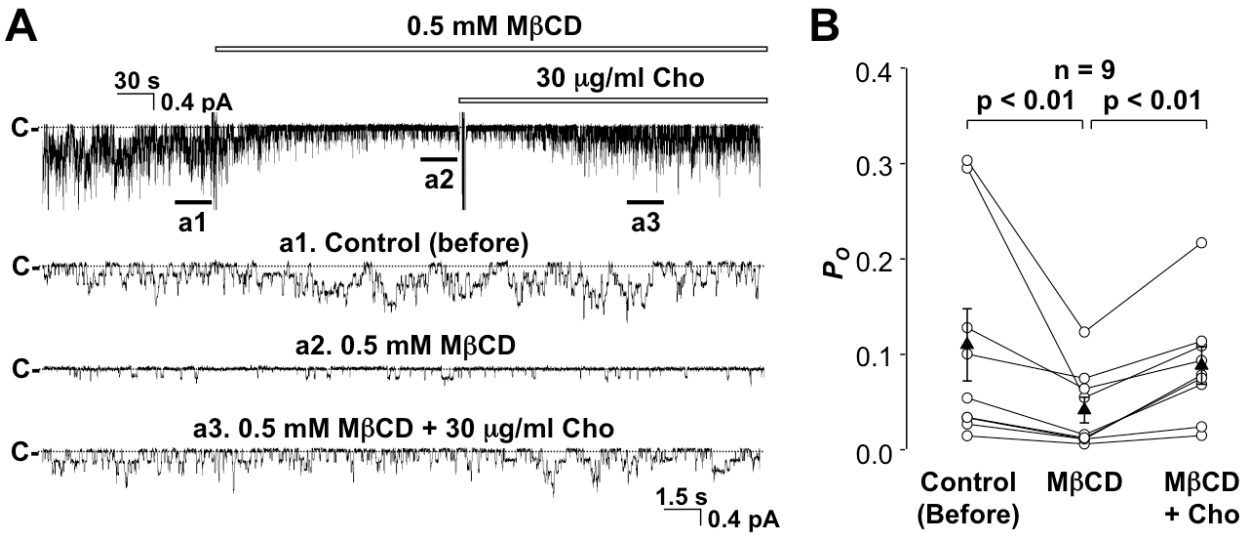

Figure 7. Cholesterol in the inner (cytoplasmic) leaflet of the apical membrane is required for ENaC P_O. (A) A representative inside-out patch showed that ENaC activity was reduced by addition of MβCD (0.5 mM) into the cytoplasmic bath; the reduction was reversed by addition of cholesterol (30 μg/ml) into the cytoplasmic bath. *"a1, a2, and a3"* are zoom-in views of the channel openings (downward events). **(B)** Summary plots of ENaC P_O under control condition (before), after addition of MβCD, or after addition of cholesterol in the presence of MβCD to the cytoplasmic bath. Figure provided by S. Wei and C. Chou.

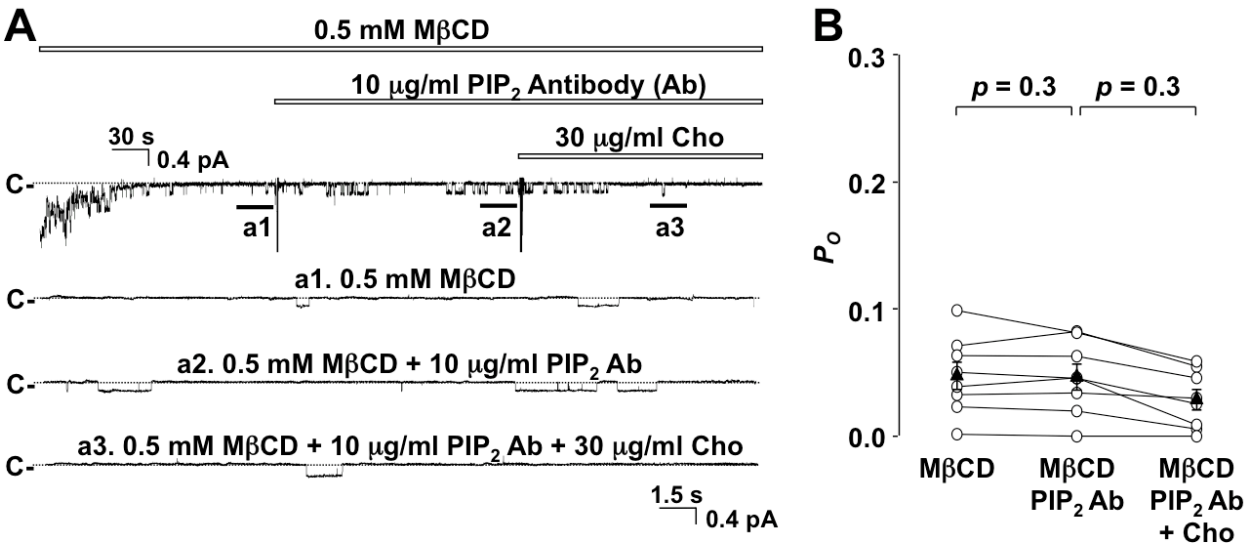

Figure 8. Sequestration of PIP_2 with its antibody abolishes the elevation of ENaC P_O by cholesterol. (A) A representative inside-out patch shows that ENaC activity was reduced after addition of MβCD (0.5 mM) into the cytoplasmic bath; after sequestration of PIP_2 with anti-PIP_2 antibody the reduction was not reversed by addition of cholesterol (30 μg/ml) into the cytoplasmic bath. *"a1, a2, and a3"* are zoom-in views of the channel openings (downward events). **(B)** Summary plots of ENaC P_O after addition of MβCD, after addition of anti-PIP_2 antibody (Ab) in the presence of MβCD, or after addition of cholesterol in the presence of both MβCD and anti-PIP_2 Ab to the cytoplasmic bath. Figure provided by S. Wei and C. Chou.

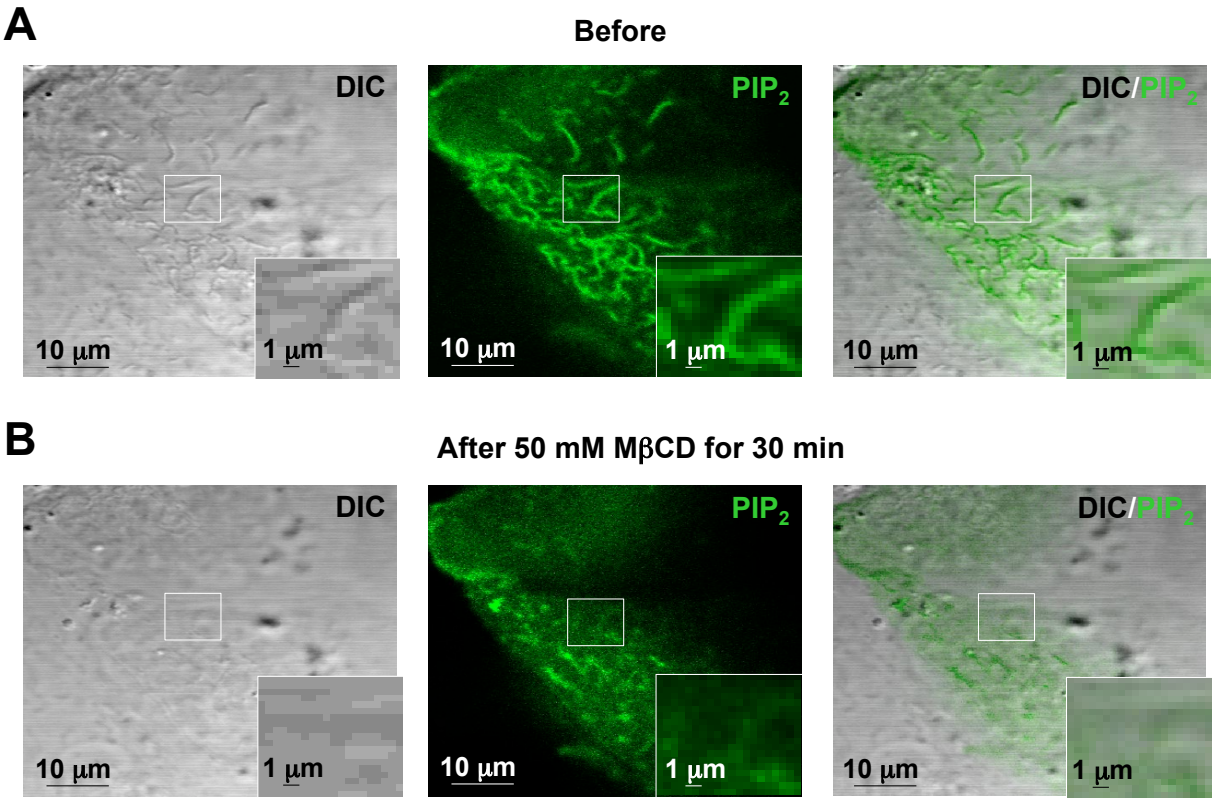

Figure 9. PIP_2 is localized in cholesterol-dependent microvilli. **(A)** Confocal microscopy images show that PIP_2 was localized in microvilli which were clearly seen in DIC and PIP_2/DIC merged images. **(B)** Confocal microscopy images show that microvilli and PIP_2 in microvilli disappeared after treatment of the cells with 50 mM MβCD for 30 min. The figures in (A) and (B) represent 15 cells from three separate experiments showing consistent results. Figure provided by S. Wei and C. Chou.

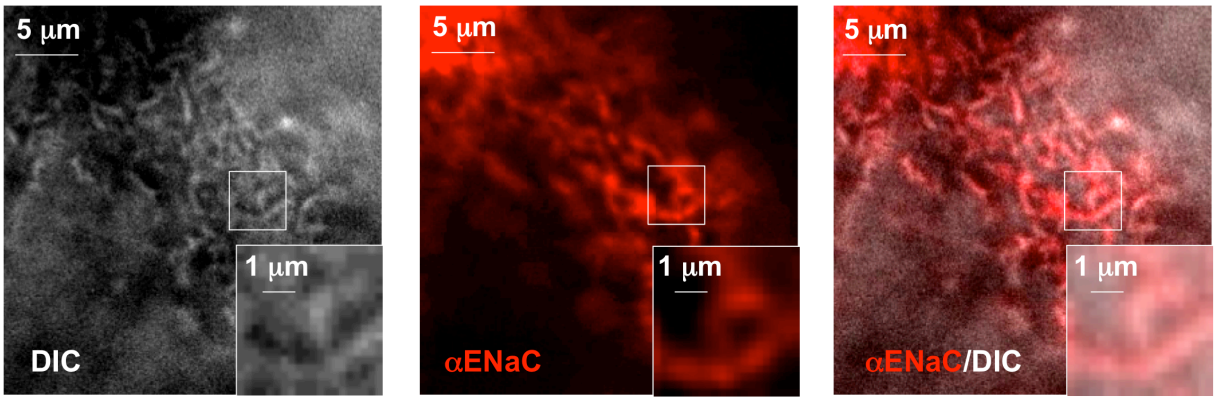

Figure 10. α-ENaC is localized in cholesterol-dependent microvilli. (A) Confocal microscopy images show that α-ENaC was localized in microvilli which were clearly seen in DIC and α -ENaC/DIC merged images. The figure represents 7 cells from three experiments showing consistent results. **(B)** Three-dimensional images from atomic force microscopy data show that microvilli disappeared after treatment of the cells with 50 mM MβCD for 30 min. The figure represents three experiments showing consistent results. Figure provided by S. Wei and C. Chou.

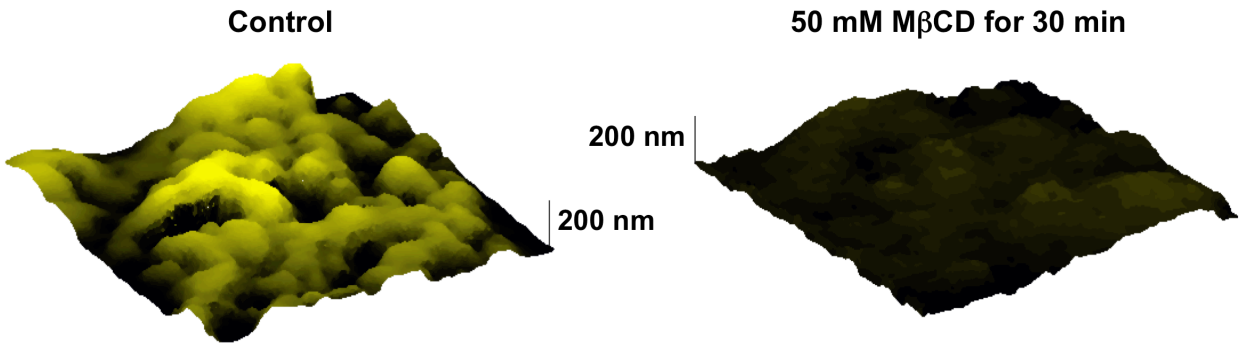

Figure 11. Microvilli structure is dependent on cholesterol. Three-dimensional images from atomic force microscopy data show that microvilli disappeared after treatment of the cells with 50 mM MβCD for 30 min. Yellow color indicates relative height measured. The figure represents three experiments showing consistent results. Figure provided by S. Wei and C. Chou.

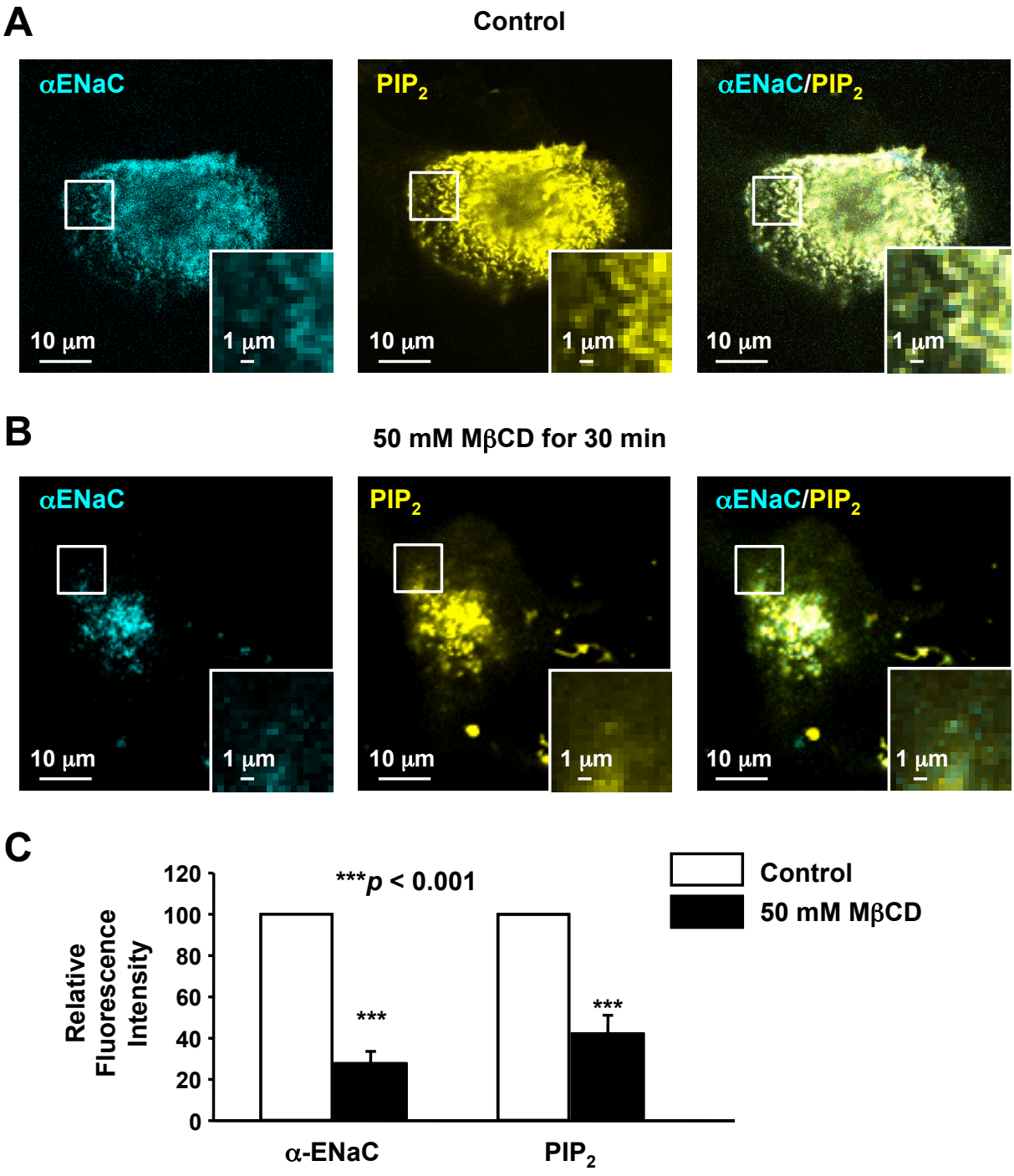

Figure 12. Extraction of cholesterol with MβCD decreases α-ENaC and PIP_2 in the apical microvillar membrane. (A) Confocal microscopy images show that α-ENaC and PIP_2 were mainly co-localized in microvilli under control conditions in mpkCCD$_{c14}$ cells **(B)** and that their

levels were significantly reduced in the cell treated with 50 mM MβCD for 30 min. **(C)** Summary plots of relative fluorescence intensity representing the levels of α-ENaC and PIP_2. Data are from 15 cells in five sets of separate experiments. Figure provided by S. Wei and C. Chou.

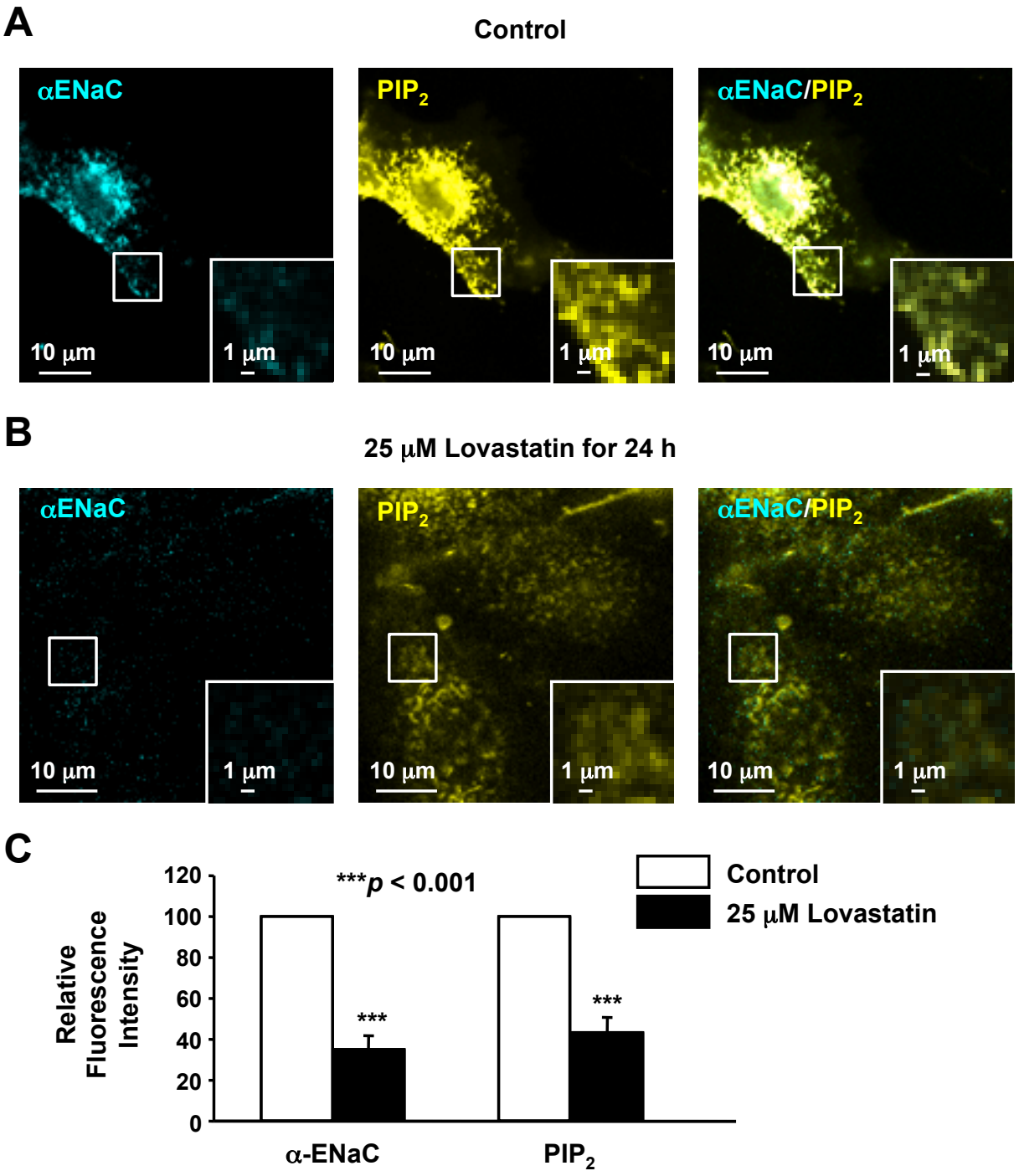

Figure 13. Inhibition of cholesterol synthesis with lovastatin decreases α-ENaC and PIP_2 in the apical microvillar membrane. (A) Confocal microscopy images show that α-ENaC and PIP_2 were mainly co-localized in microvilli under control conditions in mpkCCD_{c14} cells **(B)** and

that their levels were significantly reduced in the cell treated with 25 ¼ M lovastatin for 24 h. **(C)** Summary plots of relative fluorescence intensity representing the levels of α-ENaC and PIP_2. Data are from 15 cells in four sets of separate experiments. Figure provided by S. Wei and C. Chou.

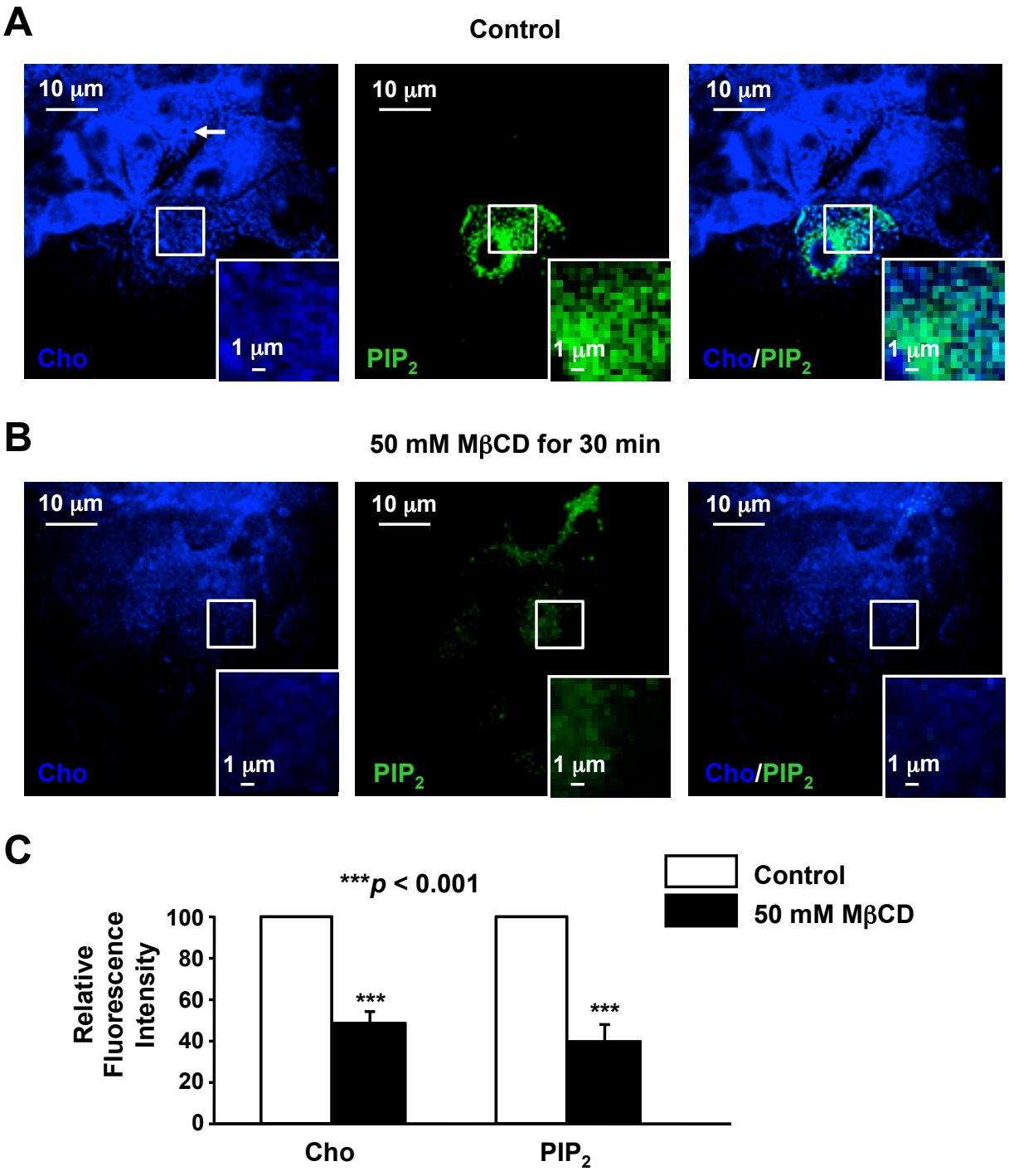

Figure 14. Cholesterol is co-localized with PIP_2 in microvilli and reduced by MβCD. (A) Confocal microscopy images show that cholesterol and PIP_2 were mainly co-localized in microvilli under control conditions **(B)** and that their levels were significantly reduced in the cell

treated with 50 mM MβCD for 30 min. **(C)** Summary plots of relative fluorescence intensity representing the levels of cholesterol and PIP_2. Data are from 15 cells in four sets of separate experiments. White arrow shows the basal body of a cilium, indicating a principal cell of the CCD. Figure provided by S. Wei and C. Chou.

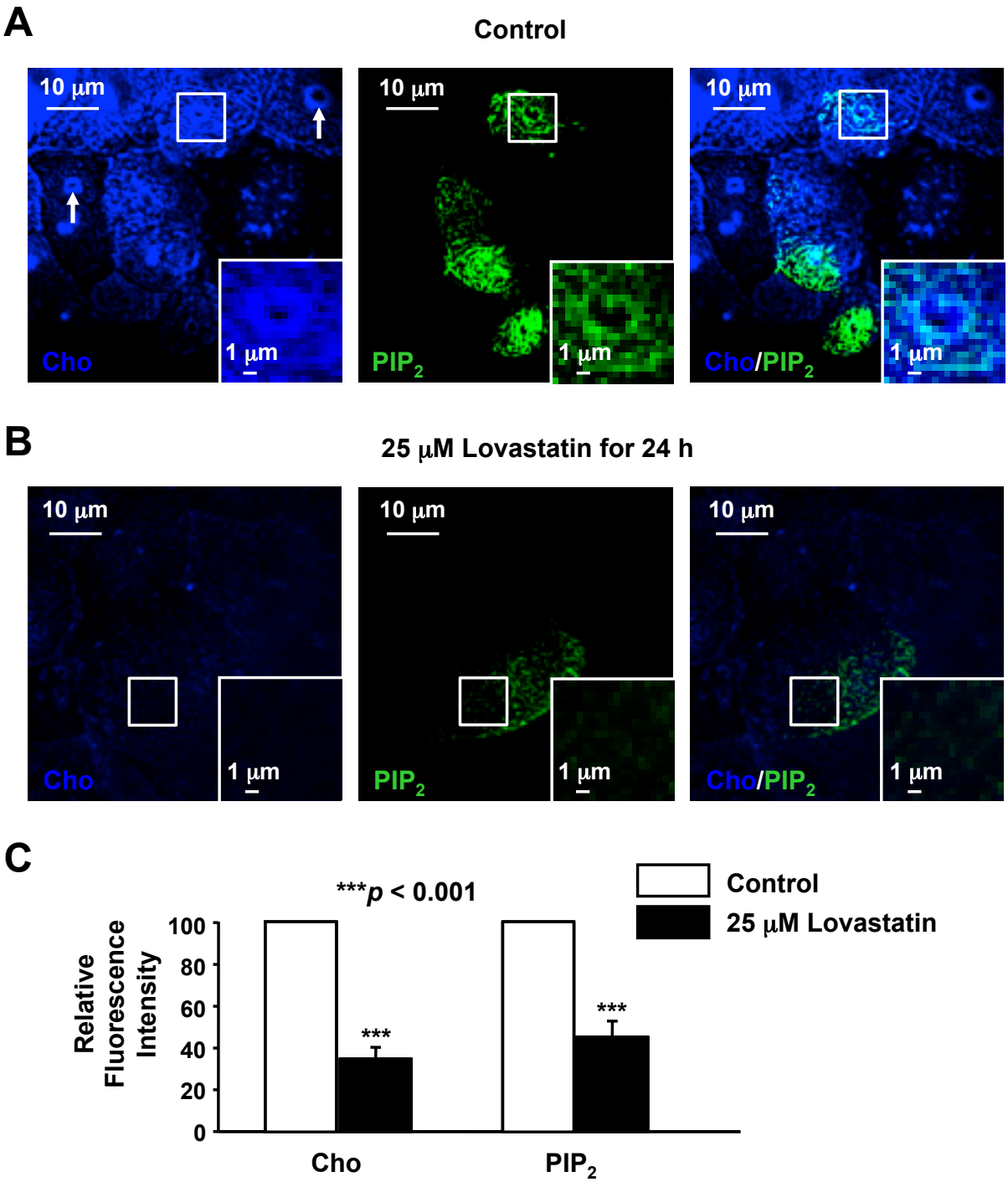

Figure 15. Cholesterol is co-localized with PIP_2 in microvilli and reduced by lovastatin. (A) Confocal microscopy images show that cholesterol and PIP_2 were mainly co-localized in microvilli under control conditions **(B)** and that their levels were significantly reduced in the cell

treated with 25 ¦M lovastatin for 24 h. **(C)** Summary plots of relative fluorescence intensity representing the levels of cholesterol and PIP_2. Data are from 15 cells in five sets of separate experiments. White arrows show the basal bodies of cilia to indicate principal cells of the cortical collecting duct. Figure provided by S. Wei and C. Chou.

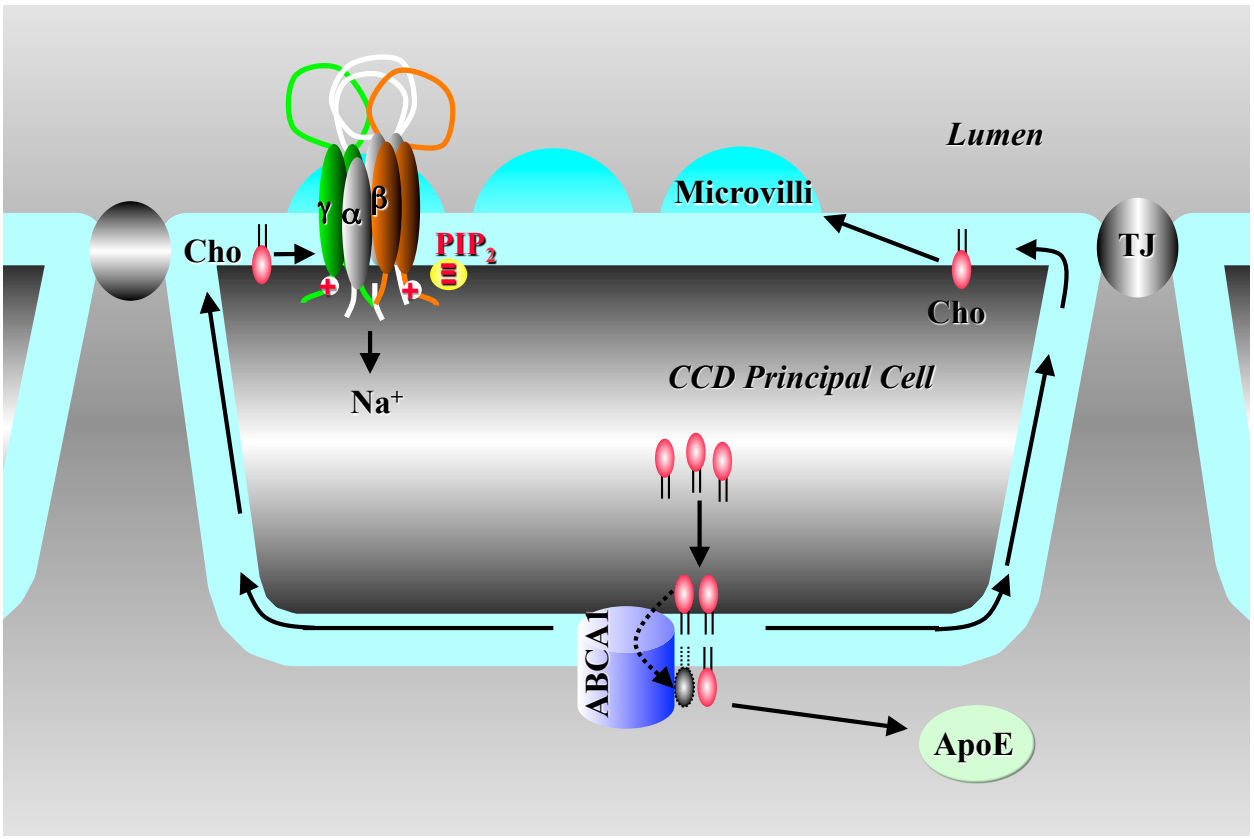

Figure 16. Proposed Schema. Cholesterol-dependent microvilli allow ENaC to associate with PIP_2 as essential for activation of ENaC and sodium reabsorption. Excessive intracellular cholesterol allows for more ENaC and PIP_2 colocalization for increased activity of ENaC and excessive sodium reabsorption.

References

1. D. C. Eaton, J. Pooler, Vander's Renal Physiology, 8e New York, NY: Mcgraw-Hill 2013.

2. C.M. Canessa, L. Schild, G. Buell, B. Thorens, I. Gautschi, J.D. Horisberger, B.C. Rossier, Amiloride-sensitive epithelial Na+ channel is made of three homologous subunits. Nature, 367**:** 463-467, 1994.

3. L. Schild, C.M. Canessa, R.A. Shimkets, I. Gautschi, R.P. Lifton, B.C. Rossier, A mutation in the epithelial sodium channel causing Liddle disease increases channel activity in the Xenopus laevis oocyte expression system. Proc Natl Acad Sci U S A, 92**:** 5699-5703, 1995.

4. R.A. Shimkets, D.G. Warnock, C.M. Bositis, C. Nelson-Williams, J.H. Hansson, M. Schambelan, J.R. Gill Jr., S. Ulick, R.V. Milora, J.W. Findling, JW, Liddle's syndrome: heritable human hypertension caused by mutations in the beta subunit of the epithelial sodium channel. Cell, 79**:** 407-414, 1994.

5. R.P. Lifton, A.G. Gharavi, D.S. Geller, Molecular mechanisms of human hypertension. Cell, 104**:** 545-556, 2001.

6. C. Saha, G.J. Eckert, W.T. Ambrosius, T.Y. Chun, M.A. Wagner, Q. Zhao, J.H. Pratt, Improvement in blood pressure with inhibition of the epithelial sodium channel in blacks with hypertension. Hypertension, 46**:** 481-487, 2005.

7. P.M. Snyder: The epithelial Na+ channel: cell surface insertion and retrieval in Na+ homeostasis and hypertension. Endocr Rev, 23**:** 258-275, 2002.

8. S.P. Wei, X.Q. Li, C.F. Chou, Y.Y. Liang, J.B. Peng, D.G. Warnock, H.P. Ma, Membrane tension modulates the effects of apical cholesterol on the renal epithelial sodium channel. J Membr Biol, 220**:** 21-31, 2007.

9. A. West, B. Blazer-Yost, Modulation of basal and peptide hormone-stimulated Na transport by membrane cholesterol content in the A6 epithelial cell line. Cell Physiol Biochem, 16**:** 263-270, 2005.

10. C. Balut, P. Steels, M. Radu, M. Ameloot, W.V. Driessche, D. Jans, Membrane cholesterol extraction decreases Na+ transport in A6 renal epithelia. Am J Physiol Cell Physiol, 290**:** C87-94, 2006.

11. N. Wang, D.L. Silver, C. Thiele, A.R. Tall, ATP-binding cassette transporter A1 (ABCA1) functions as a cholesterol efflux regulatory protein. J Biol Chem, 276**:** 23742-23747, 2001.

12. J. Wang, Z.R. Zhang, C.F. Chou, Y.Y. Liang, Y. Gu, H.P. Ma, Cyclosporine stimulates the renal epithelial sodium channel by elevating cholesterol. Am J Physiol Renal Physiol, 296**:** F284-290, 2009.

13. M. Naesens, D.R. Kuypers, M. Sarwal, Calcineurin inhibitor nephrotoxicity. Clin J Am Soc Nephrol, 4**:** 481-508, 2009.

14. Z. Ye, M.M. Wu, C.Y. Wang, Y.C. Li, C.J. Yu, Y.F. Gong, J. Zhang, Q.S. Wang, B.L. Song, K. Yu, H.C. Hartzell, D.D. Duan, D. Zhao, Z.R. Zhang, Characterization of Cardiac Anoctamin1 Ca(2)(+)-Activated Chloride Channels and Functional Role in Ischemia-Induced Arrhythmias. J Cell Physiol, 230**:** 337-346, 2015.

15. N. Yamada, H. Shimano, H. Monkuno, S. Ishibashi, T. Gotohda, M. Kawakami, Y. Wantanabe, Y. Akanuma, T. Murase, F. Takaku, Increased Clearance of Plasma Cholesterol after injection of apolipoprotein E into Watanabe heritable hyperlipidemic rabbits. PRoc. Natl. Acad. Sci, 86:665-669, 1989.

16. M. Xu, H. Zhou, Q. Gu, C. Li, The expression of ATP-binding cassette transporters in hypertensive patients. Hypertens Res, 32**:** 455-461, 2009.

17. Y. Yamada, K. Kato, T. Yoshida, K. Yokoi, H. Matsuo, S. Watanabe, S. Ichihara, N. Metoki, H. Yoshida, K. Satoh, Y. Aoyagi, A. Yasunaga, H. Park, M. Tanaka, Y. Nozawa, Association of polymorphisms of ABCA1 and ROS1 with hypertension in Japanese individuals. Int J Mol Med, 21**:** 83-89, 2008.

18. J. Gorelik, Y. Zhang, A.I. Shevchuk, G.I. Frolenkov, D. Sanchez, M.J. Lab, I. Vodyanoy, C.R. Edwards, D. Klenerman, and Y.E. Korchev, The use of scanning ion conductance microscopy to image A6 cells. Mol. Cell Endocrinol, 217:101-108, 2004.

19. P.R. Smith, A.L. Bradford, S. Schneider, D.J. Benos, and J.P. Geibel, Localization of amiloride-sensitive sodium channels in A6 cells by atomic force microscopy. Am J Physiol, 272:C1295-C1298, 1997.

20. K. Poole, D. Meder, K. Simons, and D. Muller, The effect of raft lipid depletion on microvilli formation in MDCK cells, visualized by atomic force microscopy. FEBS Lett., 565:53-58, 2004.

21. B.C. Liu, L.L. Yang, X.Y. Lu, X. Song, X.C. Li, G. Chen, Y. Li, X. Yao, D.R. Humphrey, D.C. Eaton, B.Z. Shen, and H.P. Ma, Lovastatin-induced phosphatidylinositol-4-

phosphate 5-kinase diffusion from microvilli stimulates ROMK channels. J. Am. Soc. Nephrol., 26:1576-1587, 2015.

22. J. Wang, Z.R. Zhang, C.F. Chou, Y.Y. Liang, Y. Gu, and H.P. Ma, Cyclosporine stimulates the renal epithelial sodium channel by elevating cholesterol. Am. J. Physiol Renal Physiol, 296:F284-F290, 2009.

23. H.P. Ma, S. Saxena, and D.G. Warnock, Anionic phospholipids regulate native and expressed epithelial sodium channel (ENaC). J. Biol. Chem., 277:7641-7644, 2002.

24. O. Pochynyuk, Q. Tong, J. Medina, A. Vandewalle, A. Staruschenko, V. Bugaj, and J.D. Stockand, Molecular determinants of PI(4,5)P_2 and PI(3,4,5)P_3 regulation of the epithelial Na^+ channel. J. Gen. Physiol, 130:399-413, 2007.

25. G. Yue, B. Malik, G. Yue, and D.C. Eaton, Phosphatidylinositol 4,5-bisphosphate (PIP_2) stimulates epithelial sodium channel activity in A6 cells. J. Biol. Chem, 277:11965-11969, 2002.

26. H.P. Ma, C.F. Chou, S.P. Wei, and D.C. Eaton, Regulation of the epithelial sodium channel by phosphatidylinositides: experiments, implications, and speculations. Pflugers Arch, 455:169-180, 2007.

27. Z.R. Zhang, C.F. Chou, J. Wang, Y.Y. Liang, and H.P. Ma, Anionic phospholipids differentially regulate the epithelial sodium channel (ENaC) by interacting with ✔, ☆, and ■ ENaC subunits. Pflugers Arch, 459:377-387, 2010.

28. R.M. Henderson, J.M. Edwardson, N.A. Geisse, and D.E. Saslowsky, Lipid rafts: feeling is believing. News Physiol Sci., 19:39-43, 2004.

29. K. Simons and E. Ikonen, Functional rafts in cell membranes. Nature, 387:569-572, 1997.

30. K. Simons and E. Ikonen, How cells handle cholesterol. Science, 290: 1721-1726, 2000.

31. M.C. Giocondi, P.E. Milhiet, P. Dosset, and G.C. Le, Use of cyclodextrin for AFM monitoring of model raft formation. Biophys. J., 86:861-869, 2004.

32. J.C. Lawrence, D.E. Saslowsky, J.M. Edwardson, and R.M. Henderson, Real-time analysis of the effects of cholesterol on lipid raft behavior using atomic force microscopy. Biophys. J., 84 (2003) pp. 1827-1832, 2003.

33. C.M. Johnson, G.R. Chichili, and W. Rodgers, Compartmentalization of phosphatidylinositol 4,5-bisphosphate signaling evidenced using targeted phosphatases. J. Biol. Chem., 283:29920-29928, 2008.

34. J. Maleth, S. Choi, S. Muallem, and M. Ahuja, Translocation between PI(4,5)P_2-poor and PI(4,5)P_2-rich microdomains during store depletion determines STIM1 conformation and Orai1 gating. Nat. Commun., 5:5843, 2014.

35. J. Wang and D.A. Richards, Segregation of PIP_2 and PIP_3 into distinct nanoscale regions within the plasma membrane. Biol. Open., 1:857-862, 2012.

36. M. Edidin, The state of lipid rafts: from model membranes to cells. Annu. Rev. Biophys. Biomol. Struct., 32:257-283, 2003.

37. D. Lingwood and K. Simons, Lipid rafts as a membrane-organizing principle. Science, 327:46-50, 2010.

38. Lu, M, Wang, J, Jones, KT, Ives, HE, Feldman, ME, Yao, LJ, Shokat, KM, Ashrafi, K, Pearce, D: mTOR complex-2 activates ENaC by phosphorylating SGK1. J Am Soc Nephrol, 21**:** 811-818, 2010.

39. J.M. Timmins, J.Y. Lee, E. Boudyguina, K.D. Kluckman, L.R. Brunham, A. Mulya, A.K. Gebre, J.M. Coutinho, P.L. Colvin, T.L. Smith, M.R. Hayden, N. Maeda, J.S. Parks, Targeted inactivation of hepatic Abca1 causes profound hypoalphalipoproteinemia and kidney hypercatabolism of apoA-I. J Clin Invest, 115**:** 1333-1342, 2005.

40. R.D. Nelson, P. Stricklett, C. Gustafson, A. Stevens, D. Ausiello, D. Brown, D.E. Kohan, Expression of an AQP2 Cre recombinase transgene in kidney and male reproductive system of transgenic mice. Am J Physiol, 275**:** C216-226, 1998.

41. D. Ahn, Y. Ge, P.K. Stricklett, P. Gill, D. Taylor, A.K. Hughes, M. Yanagisawa, L. Miller, R.D. Nelson, D.E. Kohan, Collecting duct-specific knockout of endothelin-1 causes hypertension and sodium retention. J Clin Invest, 114**:** 504-511, 2004.

42. H.F. Bao, T.L. Thai, Q. Yue, H.P. Ma, A.F. Eaton, H. Cai, J.D. Klein, J.M. Sands, D.C. Eaton, ENaC activity is increased in isolated, split-open cortical collecting ducts from protein kinase Cα knockout mice. American Journal of Physiology-Renal Physiology, 306**:** F309-F320, 2014.

43. P.R. Grimm, R. Coleman, E. Delpire, P.A. Welling, Constitutively Active SPAK Causes Hyperkalemia by Activating NCC and Remodeling Distal Tubules. J Am Soc Nephrol, 28**:** 2597-2606, 2017.

44. H.F. Bao, T.L. Thai, Q. Yue, H.P. Ma, A.F. Eaton, H. Cai, J.D. Klein, J.M. Sands, D.C. Eaton, ENaC activity is increased in isolated, split-open cortical collecting ducts from protein kinase Calpha knockout mice. Am J Physiol Renal Physiol, 306**:** F309-320, 2014.

45. H.F. Bao, Z.R. Zhang, Y.Y. Liang, J.J. Ma, D.C. Eaton, and H.P. Ma, Ceramide mediates inhibition of the renal epithelial sodium channel by tumor necrosis factor-✔ through protein kinase C, Am. J. Physiol Renal Physiol 293 (2007) p. F1178-F1186.

46. M. Bens, V. Vallet, F. Cluzeaud, L. Pascual-Letallec, A. Kahn, M.E. Rafestin-Oblin, B.C. Rossier, and A. Vandewalle, Corticosteroid-dependent sodium transport in a novel immortalized mouse collecting duct principal cell line. J. Am. Soc. Nephrol., 10:923-934, 1999.

47. M.N. Helms, L. Liu, Y.Y. Liang, O. Al-Khalili, A. Vandewalle, S. Saxena, D.C. Eaton, and H.P. Ma, Phosphatidylinositol 3,4,5-trisphosphate mediates aldosterone stimulation of epithelial sodium channel (ENaC) and interacts with ■ENaC. J. Biol. Chem., 280:40885-40891, 2005.

48. B.C. Liu, X, Song, X.Y. Lu, C.Z. Fang, S.P. Wei, A.A. Alli, D.C. Eaton, B.Z. Shen, X.Q. Li, H.P. Ma, Lovastatin attenuates effects of cyclosporine A on tight junctions and apoptosis in cultured cortical collecting duct principal cells. Am J Physiol Renal Physiol, 305**:** F304-313, 2013.

49. S. Rust, M. Rosier, H. Funke, J. Real, Z. Amoura, J.C. Piette, J.F. Deleuze, H.B. Brewer, N. Duverger, P. Denefle, and G. Assmann, Tangier disease is caused by mutations in the gene encoding ATP-binding cassette transporter 1. Nat. Genet., 22:352-355, 1999.

50. N. Wang, D.L. Silver, C. Thiele, and A.R. Tall, ATP-binding cassette transporter A1 (ABCA1) functions as a cholesterol efflux regulatory protein. J. Biol. Chem., 276:23742-23747, 2001.

51. A.M. Marzesco, M. Wilsch-Brauninger, V. Dubreuil, P. Janich, K. Langenfeld, C. Thiele, W.B. Huttner, and D. Corbeil, Release of extracellular membrane vesicles from microvilli of epithelial cells is enhanced by depleting membrane cholesterol. FEBS Lett., 583:897-902, 2009.

52. T. Laux, K. Fukami, M. Thelen, T. Golub, D. Frey, and P. Caroni, Gap43, marcks, and cap23 modulate PI(4,5)P_2 At plasmalemmal rafts, and regulate cell cortex actin dynamics through a common mechanism. Journal of Cell Biology, 149(7):1455-72, 2000.

53. L.J. Pike and J.M. Miller, Choesterol depletion delocalizes phosphatidylinositol bisphosphate and inhibits hormone-stimulated phosphatidylinositol turnover. Journal of Biological Chemistry, 273(35):22298-304, 1998.